Accepted Manuscript

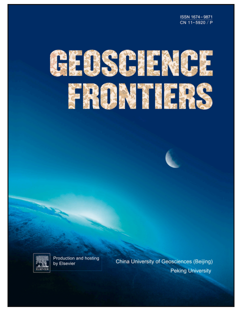

Campaign-style U-Pb titanite petrochronology; along-strike variations in timing of metamorphism in the Himalayan Metamorphic Core

Catherine M. Mottram, John Cottle, Andrew Kylander-Clark

PII: S1674-9871(18)30206-8

DOI: 10.1016/j.gsf.2018.09.007

Reference: GSF 762

To appear in: *Geoscience Frontiers*

Received Date: 15 February 2018

Revised Date: 24 July 2018

Accepted Date: 27 September 2018

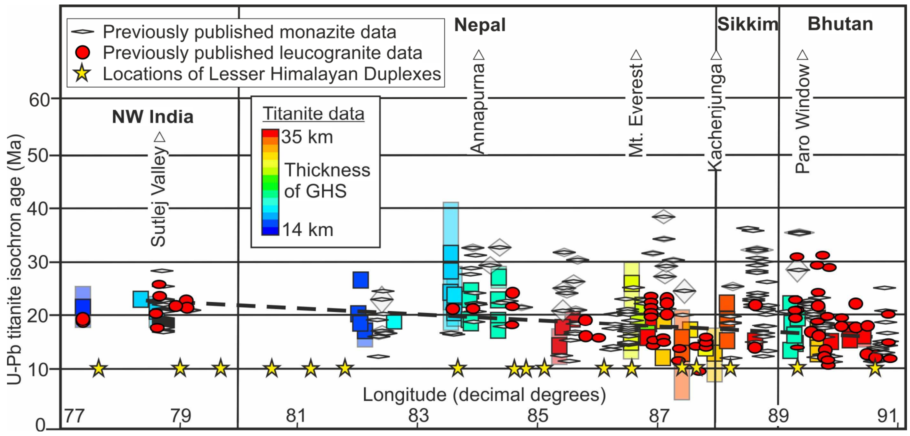
Previously published monazite data
Previously published leucogranite data
Locations of Lesser Himalayan Duplexes
Nepal
Sikkim
Bhutan
NW India
Sutlej Valley
Annapurna
Mt. Everest
Kachenjunga
Paro Window
Titanite data
35 km
Thickness of GHS
14 km
U-Pb titanite isochron age (Ma)
Longitude (decimal degrees)
0
10
20
30
40
50
60
77
79
81
83
85
87
89
91

Campaign-style U-Pb titanite petrochronology; along-strike variations in timing of metamorphism in the Himalayan Metamorphic Core.

Catherine M. Mottram[a,*], John Cottle[b], and Andrew Kylander-Clark[b]

[a]*School of Earth and Environmental Sciences, University of Portsmouth, Portsmouth, U.K.*

[b]*Department of Earth Science, University of California, Santa Barbara, 93106-9630, United States*

***Corresponding author. E-mail:** *catherine.mottram@port.ac.uk*

ABSTRACT

Present-day along-strike heterogeneities within the Himalayan orogen are seen at many scales, from variations within the deep architecture of the lithospheric mantle, to differences in geomorphologic surface processes. Here, we present an internally consistent petrochronologic dataset from the Himalayan metamorphic core (HMC), in order to document and investigate the causes of along-strike variations in its Oligocene–Miocene tectonic history. Laser ablation split-stream analysis was used to date and characterise the geochemistry of titanite from 47 calc-silicate rocks across >2000 km along the Himalaya. This combined U-Pb–REE–Zr single mineral dataset circumvents uncertainties associated with interpretations based on data compilations from different studies, mineral systems and laboratories, and allows for direct along-strike comparisons in the timing of metamorphic processes. Titanite dates range from ~30 Ma to 12 Ma, recording (re-)crystallization between 625°C and 815°C. Titanite T-t data overlap with previously published P-T-t paths from interleaved peltic rocks, demonstrating the usefulness of titanite petrochronology for recording the metamorphic history in lithologies not traditionally used for thermobarometry. Overall the data indicate a broad eastward-younging trend along the orogen. Disparities in the duration and timing of metamorphism within the HMC are best explained by along-strike variations in the position of ramps on the basal detachment

controlling a two-stage process of preferential ductile accretion at depth followed by the formation of later upper-crust brittle duplexes. These processes, coupled with variable erosion, resulted in the asymmetric exhumation of a younger, thicker crystalline core in the eastern Himalaya.

Keywords: Himalaya; Petrochronology; Titanite; Metamorphic petrology

1. INTRODUCTION

1.1 Along-strike variations in the Himalaya

The India-Asia collision has produced one of the largest and most laterally continuous mountain belts on Earth today. Plate reconstructions indicate that the counterclockwise rotation of India into Asia resulted in an oblique collision with along-strike variations in the amount of shortening and rate of collision, both of which increase from west to east (Molnar and Tapponier, 1975; Klootwijk et al., 1985; Treloar and Coward, 1991; Banerjee et al., 2008; Molar and Stock, 2009; Replumaz et al., 2010). Along-strike heterogeneities are present in the Himalaya in various forms, from the strength and geometry of the lithospheric mantle (Gahalaut and Kundu, 2012; Hammer et al., 2013; Chen et al., 2015; Hetényi et al., 2016; Webb et al., 2017), to the geometry of orogen-defining structures (Robert et al., 2011; Gibson et al., 2016; Mercier et al., 2017), to differing amounts of strain accommodated by shortening (Long et al., 2011; Burgess et al., 2012; Hirschmiller et al., 2014). Moreover, surface processes, such as the amount of precipitation and changes in surface topography also vary across the range (Duncan et al., 2003; Bookhagen and Burbank, 2010; Thiede and Ehlers, 2013; Harvey et al., 2015; Adams et al., 2016; Van der Beek et al., 2016).

The Himalayan metamorphic core (HMC) provides the key to understanding the mechanisms controlling long-term lateral variations in the orogen's collisional history. This high-grade package of metamorphic and igneous rocks records the Pressure-Temperature-time-Deformation (P-T-t-D) history of the orogen from the Eocene to present (see Kohn, 2014 for review). The HMC is often described as a continuous unit that experienced a similar along-strike tectonothermal history (e.g. Hodges, 2000). There have been a variety of models proposed to describe the mechanism(s) by which the ductile HMC was emplaced during the Miocene (e.g. see Cottle et al., 2015a for review), including end-member models of channel flow (e.g. Beaumont et al., 2001) and critical taper-type wedge models (e.g. Robinson et al., 2006; Kohn, 2008). In these models, extrusion of the HMC southward from beneath the Tibetan plateau is either controlled by gravity driven mid-crustal lateral flow (e.g. Grujic et al., 1996; Jamieson et al., 2006), or by foreland propagating thrust stacks (Davis et al., 1983). New data about the evolution of the Himalayan system through time, however, have led to the development of hybrid channel flow-wedging-type models in which the system is largely controlled by rheologic changes that migrate between these end-member states through space and time (e.g. Jamieson and Beaumont, 2013; Cottle et al., 2015a; Larson et al., 2015).

Petrochronology is the geochronological approach were ages of minerals are linked to geological processes through combined detailed petrology, microstructural analysis, geochemical characterization, and radiometric dating (Engi et al., 2017). The recent explosion of petrochronological data from different transects along the length of the orogen has revealed significant complexity and heterogeneity within the HMC (e.g. Kohn, 2014; Goscombe et al., 2018 and references therein). For example, when data from the entire HMC are compared, there are differences in the duration of metamorphism, conditions of metamorphism, presence or absence of intra-formational shear zones, unit thickness, thrusting and exhumation history between sections (Goscombe et al., 2018 and references therein). Four broad factors have been invoked to explain these along and across-strike variations, including (1) the influence of the geometry of the Main Himalayan Thrust (e.g. Robert et al., 2011), (2) tectonometamorphic discontinuities (i.e. intra-HMC structures) within the HMC (e.g. Larson and Cottle, 2014;

Montimoli et al., 2015), (3) the effect of inherited basement structures on Himalayan structures (Godin et al., 2018) and (4) variations in ductile accretion mechanisms of rock into the HMC through time and space (Larson et al., 2015; Mercier et al., 2017).

1.1.1 Geometry of the Main Himalayan Thrust

The Main Himalayan Thrust (MHT) is the main thrust-sense decollement that has controlled the accommodation of deformation during the India-Asia collision (Hauck et al., 1998). Along-strike variations in its geometry, and particularly the locations of ramps (Berger et al., 2004; Jouanne et al., 2004; Robert et al., 2011; Coutand et al., 2014; Singer et al., 2017) have been proposed as a major cause of lateral variations within the orogen. Evidence from geological studies (Larson et al., 2015; Martin et al., 2015; Gibson et al., 2016; Godin et al., 2018), as well as those using 3D shear velocity imaging (Singer et al., 2017), gravity anomalies (Hetenyi et al., 2016), thermochronological modelling (Robert et al., 2011; Coutand et al., 2014), and geomorphological investigation (Duncan et al., 2003; Bookhagen and Burbank, 2010; Thiede and Ehlers, 2013; Harvey et al., 2015; Adams et al., 2016; Van der Beek et al., 2016), all support a model in which along-strike differences in the geometry of the MHT control variations in topography, seismic activity, the development of duplexes, tectonic windows, and high-grade metamorphic processes along-strike. The geometry and position of ramps on the MHT are also key factors for controlling the thickness of the HMC (Robert et al., 2011; Gibson et al., 2016; Mercier et al., 2017; Godin et al., 2018).

1.1.2 HMC tectonometamorphic discontinuities

Tectonometamorphic discontinuities have been recognized within the GHS in several locations along the strike of the Himalayan orogen (see Montomoli et al., 2015 and Carosi et al., 2017 for review). These are generally interpreted to represent both out-of-sequence (e.g. the Kakthang Thrust in Bhutan; Daniel et al., 2003) and in-sequence structures (e.g. Kalopani shear zoning in the Kali Gandaki, Carosi et al., 2016). The apparent lateral continuity of these structures has led to the suggestion that the mid-crustal tectono-metamorphic discontinuities within the HMC form a continuous structure along the length of the orogen (Carosi et al., 2017). Such tectonometamorphic discontinuities have been identified more often by discrete breaks in geochronological and thermobarometric data rather than structural field-data controls. For example, both the Laya thrust in Bhutan (Warren et al., 2011), and the intra-GHS structure within the Sikkim HMC are mapped on P-T-t constraints alone (Rubatto et al., 2013).

1.1.3 Inherited basement structures

Major NE-trending Pre-Cambrian basement ridges are present beneath the Himalayan front within the Indian basement (Godin and Harris, 2004; Godin et al., 2018 and references therein). Variations in the timing and conditions of both deep metamorphic (Gibson et al., 2015) and surface processes (Harvey et al., 2015) within different HMC transects separated by these basement ridges may be explained by strain partitioning along pre-existing crustal weaknesses. The potential for reactivation of basement ridges and deep-seated structures has been postulated as a mechanism for causing along-strike differences in ramp and flat geometries on the MHT, thus segmenting the orogen (Godin et al., 2018).

1.1.4 Ductile accretion mechanisms

Recent work reconstructing the detailed deformation and thrusting history of the HMC has revealed significant complexity within the timing and duration of thrusting (e.g. Larson et al., 2017 and references therein). The 'integrated imbricate thrust system model' of Larson et al., (2015) demonstrates how the geometry of the basal detachment (i.e. the paleo MHT) within the orogenic system may control the development of HMC. Subcretion of rock by ductile accretion of footwall material to the hanging wall occurs along ramps on the MHT throughout the Miocene in this model. This idea is supported by thermo-numerical models simulating material accreted along transient ramps on the MHT that migrate from the foreland of the orogen to the hinterland of the orogen (Mercier et al., 2017).

1.2 Application of titanite petrochronology in the Himalayan metamorphic core

Similarities in the largely meta-sedimentary and igneous lithologies present within the HMC (e.g. DeCelles et al., 2016; Martin, 2017a) allow for comparison of orogen-controlling processes along-strike. Previous work has demonstrated that the ages of: metamorphism (e.g. Guillot et al., 1999; Goscombe et al., 2018), partial melting and leucogranite formation (e.g., Searle and Godin, 2003; Lederer et al., 2013), as well as cooling and exhumation (Warren et al., 2014; Webb et al., 2017), decrease from dominantly Oligocene-early Miocene ages in the west, to mid-late Miocene ages in the east. Because of the scale of the Himalaya and difficulties in collecting enough samples from multiple transects along-strike, this trend has previously been inferred by comparing dates from different mineral systems (e.g. zircon U-Pb, monazite Th/Pb, muscovite $^{40}Ar/^{39}Ar$), from several different studies (Guillot et al., 1999; Searle and Godin, 2003; Warren et al., 2014; Gibson et al., 2016; Goscombe et al., 2018). If real, this trend is significant because it reflects fundamental along-strike variation in the underlying processes that control mountain-building at the orogen-scale. This study aims to test both along-strike variations and intra-formational complexities in the timing of deformation in the HMC using a single mineral: titanite.

Titanite-bearing calc-silicate rocks are found along the entirety of the Himalayan mountain belt, but remain a relatively understudied resource, holding potentially valuable information about the timing and conditions of metamorphism, as well as the role of fluids during metamorphism (Groppo et al., 2013a; Rolfo et al., 2017). These rocks represent an untapped resource to investigate along-strike temporal and thermal variations in the evolution of the HMC. Titanite petrochronology is a new and fast-developing method that has the potential to become an extremely useful tool for providing timing constraints to tectonic problems (e.g. Spencer et al., 2013; Stearns et al., 2016; Kohn, 2017), directly recording both temperature (T; Zr-in-titanite thermometer of Hayden et al., 2008), and timing (t) of (near peak) metamorphism via U-Pb geochronology (Kohn, 2017). Despite several recent papers applying titanite petrochronology to a variety of lithologies (Kohn and Corrie, 2011; Gao et al., 2012; Spencer et al., 2013; Stearns et al., 2015; Garber et al., 2017; Walters and Kohn, 2017), no study has systematically addressed the role of bulk composition on titanite petrochronology. We therefore employ a 'campaign-style' approach (Spencer et al., 2013), utilizing 47 titanite-bearing samples representing a >2000 km long orogen-parallel transect along the HMC, analysed during only two analytical periods, to produce the largest, most regionally-extensive and only "internally-consistent" dataset to date. This dataset reveals the petrochronological complexities of titanite from the grain- to orogen-scale, allowing us to evaluate the role of titanite as a petrochronometer as well as the tectonic significance of the titanite U-Pb dates. Broadly, the dataset clearly shows an eastward-younging trend in the thermo-tectonic evolution of the core of the Himalayan orogen. The corroboration of this trend both validates the approach of combining methods and datasets to show orogen-scale age trends, and demonstrates the usefulness of titanite for recording T-t information in metamorphic rocks. By comparing the timing and conditions of metamorphism from a single mineral-system along-strike, it is possible to interpret large-scale, long-term variations in mid-crustal processes throughout the orogen, and ultimately provide insight into the processes controlling crustal extrusion in large hot orogens.

2. GEOLOGICAL SETTING

The Greater Himalayan Sequence (GHS) dominates the HMC (Figure 1). During the on-going Himalayan orogeny (Najman et al., 2010 for review), the GHS was subducted into the India-Asia collisional zone, deformed, partially melted and extruded between the two bounding structures, the Main Central Thrust (MCT) and South Tibetan Detachment (STD). While there has been some debate about the definition of the MCT, herein we use the protolith boundary between the Lesser and Greater Himalayan Sequence (defined by largely by detrital zircon and εNd data), in addition to the presence of a thrust-sense shear zone to define the MCT (e.g. Martin, 2017b). These structures separate GHS metasedimentary (largely pelitic, calc-silicate and quartzite) and orthogneiss units, from the underlying largely metasedimentary Lesser Himalayan Sequence (LHS) and overlying (meta)sedimentary Tethyan Sedimentary Sequence

(TSS; e.g. Hodges, 2000 for review). The presence of a weak, partially-melted, extruding GHS is central to many continental-collision evolution models (see Cottle et al., 2015a for review), and the GHS has therefore been the focus of many petrochronological studies to constrain the temperature-time evolution of the rocks to test proposed tectonic models (Kohn, 2014 for review).

For this study 47 samples, collected by 18 different geologists (see acknowledgments), were analysed from various structural levels along >2000 km of the GHS from NW India to central Bhutan (Fig. 1; Table 1). A further 12 samples were analysed, but titanite yielded very low U and/or high common Pb content and were therefore not possible to date. Below, a brief geologic context is given for each sampled region.

The most westerly calc-gneiss samples (samples beginning K09-), located in the Sutlej Valley (Fig. 1a) experienced pro-grade to peak metamorphic conditions of ~630–700°C and 0.8 GPa (Vannay and Grasemann, 1998; Walker et al., 1999) between ~35 Ma and 24 Ma, undergoing anatexis between ~22 Ma and 19 Ma (Langille et al., 2012; Lederer et al., 2013).

In far-western Nepal both the GHS and STD form klippen (DeCelles et al., 1998; Robinson et al., 2006; He et al., 2015; Braden et al., 2017; La Roche et al., 2018). Sampled calc-gneiss and impure marble samples from the Dadeldhura klippe (samples beginning DH-), and the Mugu-Karnali (samples D13-49; Fig. 1b) area experienced peak metamorphic conditions of ~690–700°C and 0.7 GPa between ~23 Ma and 18 Ma (Montomoli et al., 2013).

Calc-gneiss samples from the Kali Ghandaki valley (samples beginning P12/- and KL), the Modi Khola valley (samples beginning MK-) and the Marsyangdi valley (samples 402060–63) in the Annapurna Himalaya (Figure 1c) experienced a protracted history of prograde to peak metamorphism between ~49 Ma and 20 Ma at metamorphic conditions of ~600–800°C and 0.8–1 GPa (Vannay and Hodges, 1996; Catlos et al., 2001; Martin et al., 2010; Corrie and Kohn, 2011; Kohn and Corrie et al., 2011; Carosi et al., 2015; Parsons et al., 2016a,b).

Calc-silicate boudins within kyanite-sillimanite bearing meta-pelite samples were collected from the lower and upper GHS in the Langtang Valley (samples beginning 14-; Fig. 1d) structurally above the Langtang Thrust. These rocks experienced metamorphic conditions of 1 GPa and <700°C during prolonged deformation between ~35 Ma and 15 Ma (Kohn et al., 2004).

Samples from the Mt. Everest transect include calc-gneisses from the lower GHS in the proximal hanging wall of the MCT and the upper GHS near the large leucogranite bodies in the vicinity of Mt. Everest. Calc-schist and amphibolite samples were also analysed from the Hermit's gorge and Rongbuk Monastery sections of the Rongbuk glacier in the immediate footwall of the STD (samples beginning R03-; Fig. 1e). These rocks experienced prograde-peak metamorphism between ~38 Ma and ~25–16 Ma (Simpson et al., 2000; Viskupic et al., 2005; Jessup et al., 2008; Cottle et al., 2009, 2015b) at ~700°C and 0.5–0.6 GPa in the GHS (Searle et al., 2003), which reduce to ~630°C and 0.5 GPa close to the STD (Hodges et al., 2000; Jessup et al., 2008).

Calc-gneisses found as metre-scale boudins within the lower GHS, pelite assemblages, and as tens to hundreds-metre thick bodies associated with marbles in the upper GHS rocks, were sampled from far-eastern Nepal (samples 05-55; 12:65 etc; Figure 1f). In the upper levels of the GHS peak metamorphism occurred at conditions of ~800°C and 0.8–1 GPa (Groppo et al., 2009) at ~18 Ma (Struele et al., 2010), with later decompression-related melt crystallisation at ~750–800°C and 0.4–0.5 GPa (Groppo et al., 2013b) at ~16 Ma (Struele et al., 2010).

Calc-silicate boudins from the GHS of the Sikkim Himalaya (samples beginning SK12-; Fig. 1g) experienced peak metamorphic conditions of ~670–800°C and 0.8–1 GPa between ~26 Ma and19.5 Ma (Dasgupta et al., 2004; Mottram et al., 2014; 2015a).

Titanite-bearing amphibolite, impure marble and calc-gneiss rocks (samples DRB 1213, 1219 and 1233, CWB-10-2, TH-B12-1605) were sampled from migmatitic gneiss of western Bhutan (Fig. 1h). This area is affected by the out-of-sequence Laya thrust (i.e. Warren et al., 2011), and two N-S trending normal fault systems, the Yadong-Gulu cross structure and the Lingtse Fault (Cooper et al., 2015). The host rocks experienced prograde to peak metamorphic conditions between ~36 Ma and 18 Ma (peak conditions of ~770°C and 0.8 GPa) in the western Jomolhari massif area and at 19.5–16.9 Ma (peak metamorphic conditions of ~800°C and >0.8 GPa) in the footwall of the Laya thrust (Regis et al., 2014).

Impure marble and calc-gneiss rocks from the upper GHS were analysed from central Bhutan (samples beginning FB-; BU- and B-; Fig. 1i). The upper GHS rocks in the Ura Klippe experienced metamorphism between ~26 Ma and 15.4 Ma at peak conditions of ~790°C and 0.9 GPa (Kellett et al., 2010).

3. SAMPLE PETROGRAPHY

In most of the 47 studied impure marble, amphibolite and calc-schist, calc-silicate and calc-gneiss samples, titanite is present as moderately large (typically of 200–1000 µm) euhedral grains that form part of the equilibrium assemblage (Figs. 1–-2). Chemical zoning was observed in a minority of crystals (Fig. 3). Detailed descriptions, petrography, photomicrographs and descriptions of reaction textures are given in Supplementary Material S1 and are briefly summarized here and in Table 1.

Calc-gneiss (n = 16) and calc-silicate (n = 12) samples with the assemblage titanite + K-feldspar + calcite + amphibole + zoizite + clinopyroxene + scapolite + plagioclase + quartz (± biotite, orthopyroxene, and garnet; Figure 2a), display granofels textures with granular interlocking grains, myrmekite textures, lobate grain boundaries indicative of grain boundary migration during high-temperature deformation. Common reaction textures in these rocks include: clinopyroxene rimmed by (1) epidote, amphibole and associated titanite (Fig. 2b), or (2) biotite, calcite, zoizite and scapolite. Garnet-clinopyroxene symplectite textures are observed in six samples (Fig. 2a). Impure marbles (n = 9) contain the assemblage titanite + zoizite + muscovite + K-feldspar, biotite + clinopyroxene, + quartz + calcite (± amphibole; Fig. 2c). Titanite is associated with clinopyroxene and zoizite breakdown in these samples. Amphibolite schists (n = 10; Fig. 2d) are defined by assemblages of titanite + biotite + plagioclase + quartz (± zoizite ± muscovite ± clinopyroxene ± amphibole), where titanite is part of an equilibrium assemblage in the matrix.

Titanite-forming reactions are strongly sensitive to the bulk composition and the CO_2 content of the rock (Groppo et al., 2017). However, titanite is generally stable at a range of CO_2 contents for the conditions of T >600°C and ~0.8–1.0 GPa experienced by these samples (Zr-in-titanite data from this study and from estimates from previously published P-T data; Table 1; Supplementary Table S3; Groppo et al., 2017). The textures observed in the samples indicate that titanite generally formed during initial decompression when peak metamorphic minerals became unstable and started to react. For example, in several samples titanite is associated with clinopyroxene break down reactions: clinopyroxene + ilmenite + quartz + H_2O = titanite + hornblende (Stephenson and Cook, 1997; Harlov et al., 2006). In lower-grade samples, such as the impure marbles, titanite likely formed from a precursor Ti-bearing phase such as rutile (e.g. rutile + calcite + quartz = titanite + CO_2; Frost et al., 2000; Mathavan and Fernando, 2001).

4. TITANITE PETROCHRONOLOGY METHODS AND RESULTS

4.1 Methods

Select titanite grains were identified through back-scatter electron microscopy and energy-dispersive spectroscopy on a FEI Q400f FEG scanning electron microscope and mapped using a Cameca SX-100 electron microprobe (EMP) at the University of California, Santa Barbara (UCSB), USA. U-Pb isotopic concentrations and trace-element compositions in titanite were analysed *in-situ* in thin section using Laser Ablation Split Stream Inductively Coupled Plasma Mass Spectrometry (LASS-ICPMS) at UCSB, following methods of Kylander-Clark et al. (2013) and Spencer et al. (2013). The Zr-in-titanite thermometer of Hayden et al., (2008) was used to calculate titanite temperatures. Full analytical conditions are described in Supplementary Material S2 and Supplementary Table S2.

4.2 U-Pb Petrochronology

Titanite U-Pb petrochonology results are summarized in Table 2, Fig. 3, and in Supplementary Tables S1 and Supplementary Material S3. Titanite $^{238}U/^{206}Pb$–$^{207}Pb/^{206}Pb$ lower intercept dates range from ~30 Ma to 12 Ma along the orogen, however, dates as young as 12 Ma are only found east of Mt. Everest.

U-Pb systematics fall into three types, with no correlation between the type of age trend and the structural or along-strike location (Fig. 3; Supplementary Material S3). (1) In 27 samples, the U-Pb data form a single population with a well-defined lower intercept date (Fig. 3a). Such samples span in age from the youngest sample 09-25 from far-eastern Nepal, that yields a date of 13.7 ± 0.5 Ma (MSWD = 0.9), to the oldest sample KL-8-11-8 from the Annapurna Himalaya at 24 ± 0.8 Ma (MSWD = 0.9). 2). (2) A further 12 samples yield a spread of dates (Fig. 3b). Lower intercept dates in these samples span ca. 14–13 Ma in sample CWB-10-2 in Bhutan, to 27–18 Ma in sample 402063 in the Annapurna Himalaya. (3) In 8 samples, a combination of low U and/or varying common Pb composition in analyses yield poorly defined U-Pb date(s), as indicated by the high MSWDs yielded in some of these sample populations (Fig. 3c). Dates within this type of sample range from ~12.4 Ma (sample 13-26 from far-eastern Nepal; MSWD = 0.8) to ~31 Ma (sample KL-4-11-5, from the Annapurna Himalaya; MSWD = 74).

Dates between 20 Ma and 30 Ma are present throughout the orogen; however, the youngest dates recovered reveal a consistent eastward-younging trend (Fig. 7). The youngest dates in each region from west to east are: ~20.5 Ma in NW India, ~18.2 Ma in central Nepal; ~15.2 Ma in the Everest region; ~14.8 Ma in Sikkim; and ~12.6 Ma in eastern Bhutan. If only samples from the structurally upper 20% of the GHS in each transect are compared, a consistent younging trend is still observed (Figure 7), where ages vary from ~22 Ma at 78° longitude to ~17–13 Ma at 90° longitude, demonstrating that this pervasive eastward-younging trend is not simply a function of sampling bias. Due to disagreements regarding how the MCT is defined along strike (see Martin, 2017b for review), and lack of suitable titanite-bearing lithologies in the immediate vicinity of the MCT, a similar comparison for the MCT is not possible.

Differing host lithologies, and coexisting phases all contribute to variable titanite REE content (Figure 3). Low count rates for trace elements in some samples also limit detection of certain elements in some samples (Supplementary Tables S1-2; Supplementary Material S3). Samples with single age populations generally show a limited spread in trace element abundances; for example, sample KL-8-11-8, from the Annapurna Himalaya, is enriched in LREE, contains a Eu anomaly and is relatively depleted in HREE (Fig. 3a). Samples that yield a spread in ages commonly also have a spread in HREE composition; e.g., Sikkim sample SK12-216 is relatively depleted in HREE in the oldest age analyses and more enriched in HREE in the youngest age analyses (Fig. 3b). Samples that contain varying amounts of common Pb generally have different REE patterns for the apparent older analyses, which in the case of sample 13-26, from far-eastern Nepal, are relatively more enriched in HREE (Fig. 3c).

4.3 Zr-in-titanite thermometry

Zr-in-titanite temperatures were calculated at pressures based on previous thermobarometrical modelling of the host rocks (Section 2; Supplementary Material S2; Supplementary Table S4). Temperatures vary from 626-814°C and there are overall no systematic variations in temperature either along or across strike (for example a decrease in temperature towards the MCT; Figs. 4–5). Temperatures range of ~657–700°C in the Sutlej valley, NW India; ~710–740°C in western Nepal; ~678–780 °C in the Annapurna area, central Nepal; ~716–785 °C Ma in Langtang valley, central Nepal; ~665–687 °C in the Everest region of central Nepal; ~686–814 °C Ma in eastern Nepal; ~742–762°C in the Sikkim Himalaya; ~716–791°C the Jomolhari area of eastern Bhutan; and ~626–730 °C Ma in central Bhutan. There is a strong correlation between lithologies and temperature; calc-gneisses yield temperatures ranging of 711–814°C, calc-silicate samples range of 657–791°C, garnet-bearing calc-gneisses range in temperatures between 686–754°C, amphibolite samples range of 665–766°C and impure marble samples range of 626–738°C.

5. DISCUSSION

5.1 Titanite Petrochronology

The large-scale titanite petrochronological dataset presented here represents several different lithologies with variations in the metamorphic reaction textures shown in the rocks. Moreover, titanite varies in grain size, elemental zoning, and U-Pb dates and trace element patterns. The details of this new dataset provides an opportunity to discuss some of the wider implications for titanite petrochronology.

5.1.1 Titanite closure temperature

The temperature at which titanite closes to thermally mediated volume diffusion of Pb has been a matter of debate for some time (as summarized by Kohn, 2017), and in empirical studies has been estimated to be >650–700°C (Scott and St-Onge, 1995; Zhang and Scharer, 1996), to as high as 800°C (Gao et al., 2012). The titanite 'Pb closure temperature' based on the Dodson approach is defined as 668°C at a cooling rate of 10°C/Ma for a spherical geometric factor and a 5 mm diffusion radius and grain diameter (Cherniak, 1993). Based on this approach, it might be reasonable to consider titanite U-Pb dates to reflect the timing of cooling (Warren et al., 2012). Increasingly, however, it is being recognized that U-Pb titanite dates instead record the timing of crystallization (e.g. Kohn, 2017; Stearns et al., 2015; 2016 and references therein). If the closure temperature concept is applicable to titanite, there should be a systematic relationship between grain size and age, with smaller grains yielding younger ages based on shorter diffusion distances. However, similar to the observation of Stearns et al., (2015), we find no such relationship. In 57% of our samples, titanite of varying grain size records a single $^{238}U/^{206}Pb$–$^{207}Pb/^{206}Pb$ isochron (Figure 3a, Supplementary Material S1). For titanite that range in size from 50 µm to –500 µm diameter, a cooling rate of 200°C/Ma is required to produce a single age by thermally-mediated diffusion (Cherniak, 1993). The typical cooling rate for rocks in the Himalaya of 50°C/Ma (Godin et al., 2001; Vannay et al., 2004; Kellett et al., 2013; Mottram et al., 2015b), is inconsistent with the diffusion-based modelled cooling rate, indicating that the single age population samples represent the timing of complete (re)crystallization of titanite. We therefore infer that the closure temperature of titanite is significantly higher than suggested by experimental data (e.g., Spencer et al., 2013).

5.1.2 Age, temperature and trace element trends

Titanite U-Pb ages from this study falls into three main trends with analyses either yielding: one age population, already discussed in the previous section (Fig. 3a); a spread between two intercepts (Fig. 3b) or; Pb isotopic signatures indicative of the influence of a non-common $^{207}Pb/^{206}Pb$ component (Fig. 3c).

In ~25% of the samples, a ~5–10 Ma spread in dates is accompanied by a spread in Zr-in-titanite temperature and REE concentrations (Figures 3b and 4). These trends can be explained by either thermally mediated volume diffusion of Pb (e.g. Scott and St-Onge 1995), or one or more phases of (re-)crystallization (e.g. Stearns et al., 2015). Zr diffusion in titanite is prohibitively slow to cause age/ temperature variations except at very high temperatures (10's of m.y. at >800°C; Kohn, 2017). Samples in this study have a maximum titanite age spread within a single sample of 10.5 Ma (sample 12-65 from eastern Nepal) and have largely experienced temperatures below 800°C (for example, temperatures range of 723–740°C ± 18°C for sample 12-65). We therefore interpret that the age spread within titanite is a result of (re)crystallization. This interpretation is supported by the observation that in samples that display a spread in age there is also distinct elemental zoning patterns and trace element patterns that covary with age, inconsistent with thermally mediated volume diffusion.

Trace-element concentrations in titanite vary significantly between samples (Supplementary Material S3). It has been demonstrated that trace element patterns in titanite can reflect interaction with fluids, melt and other minerals within the metamorphic assemblage (Garber et al., 2017). In this study, titanite with Zr-in-titanite temperature of >750°C generally have a narrower range in trace element concentrations, often with a Eu anomaly and systematic variations in either the HREE or LREE or both (for example 402060; 07-22; 12-65; CWB-10-2; TH-B12-1605; Supplementary Material S3). In contrast, samples with average Zr-in-titanite temperatures below 750°C have diffuse, scattered trace element patterns, often enriched in MREE (06-57; 10-37; DRB1219; K09-65; KL-4-11-5; R03-71; Supplementary Material S3). This difference is likely due to the relationship between temperature, Al content and trace element partitioning as highlighted by Garber et al., (2017). In some samples, younger titanite is enriched in LREE (e.g. samples CWB-10-2, DRB1233, SK12-216, TH-B12-1605 from the Bhutan Himalaya; Supplementary Material S3) and are sometimes accompanied by an enrichment in HREE (e.g. sample SK12-216 from the Sikkim Himalaya; Figure 3). This indicates either enriched whole-rock concentrations, breakdown of a LREE-bearing accessory phase(s), interaction with an enriched fluid, or an increased compatibility of such elements during (re)crystallization (Garber et al., 2017). Enrichment in Y in these samples indicates that titanite grew during post-peak metamorphism when Y was released by garnet breakdown (e.g. Kohn et al., 2005). Breakdown of other accessory phases such as xenotime, apatite or allanite could also provide trace elements on the prograde path for titanite-forming reactions, for example the release of HREE through the breakdown of xenotime (e.g. Larson et al., 2018).

Zr-in-titanite temperatures derived in this study vary through time, with temperatures both increasing and decreasing in different samples (Fig. 4). Samples that show an increase in temperature through time are interpreted to record prograde growth. For example, sample DRB1233 from western Bhutan records increasing Zr-in-titanite temperature through time (Fig. 4a). In sample DRB1233 from Bhutan, the majority of analyses overlap with interpreted prograde-peak metamorphic conditions of ~750°C between ~29 Ma and 18 Ma (Regis et al., 2014; Figs. 4 and. 6b). In sample DRB1213 from the same area in western Bhutan (Fig. 1), a decreasing temperature-time path (Fig. 4b) roughly overlaps with interpreted retrograde path post-17 Ma (Warren et al., 2012; Regis et al., 2014). Sample SK12-216 from the nearby Sikkim

Himalaya (Fig. 1), records a temperature range of ~710–810°C among individual analyses that indicates titanite growth during both heating and cooling (Fig. 4c). The age trends overlap with interpreted P-T-t paths from the area, where prograde metamorphism is recorded by monazite between ~20.7 Ma and 15.8 Ma with peak metamorphic conditions occurring at 14.5–13.1 Ma (Mottram et al., 2015a).

Nearly one fifth of all samples yield arrays in Tera-Wasserburg space consisting of one (or more) Himalayan-age discordia trajectories and a sub-vertical discordia trajectory indicating the presence of a (partially recrystallised) older component (Fig. 3c; Supplementary Material S3). These older generations of titanite also yield significantly different REE patterns, indicating that they likely crystallised under different chemical and/or physical conditions (Fig. 3c; Supplementary Material S3). We therefore infer that the titanite in these samples contains remnant Pb from older (probably Proterozoic) titanite, or other accessory phase, such as rutile, that survived several millions of years of Cenozoic metamorphism at upper amphibolite-facies conditions without equilibrating with the whole rock. This indicates that at least part of the initial titanite can survive high-temperature metamorphism; this inheritance can have a major influence on the common Pb isotopic ratios of titanite (Pidgeon et al., 1996; Zhang and Scharer, 1996; Rubatto and Hermann, 2001; Aleinikoff et al., 2002; Kylander-Clark et al., 2008; Gao et al., 2012;; Spencer et al., 2013).

5.1.2 The effect of bulk composition

The 59 samples analysed in our study (47 of which gave suitable U/Pb ratios to be successfully dated), span a range of lithologies (Table 1, Fig. 2), with 18 amphibolites (61% dating success rate), 17 calc-gneisses (100% dating success rate), 17 (garnet-bearing) calc-silicates (71% dating success rate), and 7 marbles (100% dating success rate). There appears to be a link between metamorphic reaction textures, bulk composition and type of age spectrum yielded by samples. Titanite within amphibolite samples are the least likely to yield useable ages, which we speculate may be due to low U in the protolith. For the successfully dated samples, there is a link between lithology, age spectra, Zr-in-titanite temperatures and metamorphic reaction textures present in the rocks. A higher proportion of the marble and amphibolite samples yield a single population age (90% of amphibolite samples and 56% marble samples; Table 3). Titanite within amphibolite and marble samples also yield the average lowest Zr-in-titanite temperatures of 665 ± 19°C and 626 ± 18°C respectively (Table 3). For example, amphibolite schist sample R03-40 from the Everest section yields a single age population of 18.8 ± 2.5 Ma and a temperature of 665 ± 40°C. Marble sample B126 from central Bhutan yields a single age population of 15.5 ± 0.8 Ma and a temperature of 658 ± 38°C. This is in contrast to the calc-gneiss samples, which in 50% of cases yield a spread in ages. For example, calc-gneiss sample TH-B12-1605 from western Bhutan yields a spread in ages between two intercepts at 19.1 ± 2 Ma and 15.3 ± 1.3 Ma (Supplementary Material S3). Calc-gneiss samples also yield some of the highest Zr-in-titanite temperatures of 814 ± 16°C. 50% of calc-silicate samples yield U-Pb data that indicate partial recrystallization of an older phase (Table 3).

It is postulated that in the samples with clear reaction textures, titanites may (re)crystallise by dissolution-precipitation mechanisms in the presence of fluid or melt, causing a younger (re)crystallised titanite rim (Garber et al., 2017; Stearns et al., 2016). For example, in calc-gneiss sample 402063 from the Marysangdi valley, titanite is associated with a reaction texture of clinopyroxene rimmed with epidote and amphibole (Supplementary Material S1) and yields a spread of ages between two intercepts at 27.4 ± 1.6 Ma and 18.2 ± 1.9 Ma. It could therefore be suggested that the titanite rims represent (re)crystallization during clinopyroxene breakdown reactions. In less fertile samples, such as the calcite-dominated impure marble samples, titanite is not related to reaction textures. In these samples, unfavourable bulk-compositions, or limited fluid availability, results in the titanite recording only one (re)crystallization event. It is therefore likely that the availability of fluids, the deformational history of the rock, and bulk compositions favourable for metamorphic reactions are important factors dictating the degree of age complexity observed in metamorphic titanite.

In aggregate, our empirical titanite dataset adds to the mounting evidence that the closure temperature of titanite is much higher than originally suggested (Cherniak, 1993; 2006), and is likely to be over ~700°C. Age and temperature variations preserved in crystals that have experienced metamorphism at 626-814°C indicate the prohibitively slow nature of Pb and Zr diffusion within titanite. Bulk composition, availability of fluids and deformation-related recrystallisation are likely to be key controlling factors in defining the age trends documented within titanite from metamorphic rocks.

5.2 Case study-specific implications for the HMC

Titanite in this study was analysed from eleven different transects along much of the length of the central Himalaya. Because this dataset is large and covers a significant portion of the HMC, there is merit in discussing in detail a sub-section of the transects in detail. The implications of the large-scale trends of the dataset are then discussed in the subsequent section.

5.2.1 Annapurna Himalaya

The presence of the intra-GHS Kalopani Shear zone (Carosi et al., 2016), and a long history of burial, metamorphism, partial melting and exhumation, which spans from as early as 48–18 Ma (as summarized by Carosi et al., 2015; Iaccarino et al., 2015; Larson and Cottle, 2015), make the Kali Gandaki in the Annapurna Himalaya interesting for exploring the evolution of the evolution of the HMC. The titanite data presented here spans between 31 ± 10 Ma and 20 ± 1 Ma (Tables 2 and 4; Fig. 7). U-Pb geochronology from deformed and undeformed leucogranites constrain movement on the South Tibetan Detachment system in the area to between ~22.5 Ma and 18.5 Ma (Hodges et al., 1996; Godin et al., 2001). The titanite U-Pb date of 23.4 ± 5.6 Ma from sample P12/48, located in the immediate vicinity of the STDS in the Kali

Gandaki, overlaps with the earliest period of STD movement. Structurally beneath the STD, within the upper GHS the Kalopani shear zone is interpreted to have initiated at ~41–30 Ma (Carosi et al., 2016), which is in agreement with U-Pb dates and Zr-in-titanite temperatures of 31 ± 10 Ma and 734 ± 37°C yielded here from sample KL-4-11-5 in the footwall of the Kalipani shear zone. Monazite is interpreted to have grown during peak metamorphism at ~36–28 Ma at temperatures of ~710–720°C at 1 GPa in the same area, overlapping within uncertainty with our titanite data (Iaccarino et al., 2015; Fig. 6a). On the retrograde path, rocks experienced P-T conditions of 650–670 °C and 0.7–0.8 GPa, with monazite dates spanning between ~25 and 18 Ma (Iaccarino et al., 2015). Titanite data yielded here constrains the initial part of this decompression path with U-Pb dates and Zr-in-titanite temperatures of 24 ± 0.8 Ma/ 766 ± 39°C and 20 ± 1 Ma /743 ± 40°C (samples KL-8-11-8 and P12/054 from this study; Table 2; Table 4; Fig. 6a). Collectively, this supports a prolonged period of heating and cooling within the HMC in the Annapurna Himalaya, but at relatively lower temperatures than other samples from similar structural levels along-strike in the orogen (Figure 6).

Titanite in samples from the Modi Khola also record over 10 million years of protracted crystallization during heating (Kohn and Corrie, 2011). Previous work has outlined titanite growth along a prograde path at temperatures of 700–750°C at ~37 Ma increasing to temperature of 775°C by ~24 Ma (Kohn and Corrie, 2011). Titanite in samples analyzed in this study, MK9, MK14 and MK15, from the Modi Khola record metamorphic crystallization from 24.5 ± 1.5 Ma to 18.2 ± 1.2 at temperatures of 739–780 ± 15° and therefore overlap with, and extend beyond the final stages of titanite (re)crystallization in the Kohn and Corrie (2011) study. It can be interpreted that titanite recrystallized during melt crystallization between 22-17 Ma in this section, coeval with peritectic monazite crystallising in nearby pelitic samples (Corrie and Kohn, 2011). Titanite is associated with clinopyroxene break down reactions in the samples reported herein. It can therefore be interpreted that samples do not record the older heating history either due to complete recrystallization of titanite during clinopyroxene breakdown reactions in the initial retrograde metamorphic stages, and/or due to differences in fluid-mediated dissolution-precipitation growth of titanite during the early metamorphic history. This demonstrates that samples collected from the same outcrop can record different P-T-t paths depending on the local bulk composition, availability of elements for reactions and due to fluid/ melt distribution in the rocks.

5.2.2 Everest, Nepal

In the Everest Himalaya, the South Tibetan Detachment is exposed as the Lhotse detachment. Here, the rocks have undergone sub-simple shear on the margins of the extruding GHS, (Jessup et al., 2006), during up to 170 km of movement on the STD (Law et al., 2011). There has been telescoping of the isotherms in the vicinity of the thrust, with higher flow stresses of ~25–35 MPa in the immediate 50 m vicinity of the thrust reducing to 10–15 MPa ~100–550 m beneath the fault (Law et al., 2011). Monazite from the footwall of the STD in Hermit's gorge (Fig. 7), yield a spread of dates that are interpreted to represent metamorphism at 24 Ma, and melt crystallization at 20.4 Ma (Cottle et al., 2015b). In the immediate footwall of the fault, movement on the detachment is constrained to between ~16.4 Ma and 15.4 Ma (Cottle et al., 2015b). Brittle deformation during exhumation is recorded by muscovite $^{40}Ar/^{39}Ar$ dates of ~15.5–14.2 Ma and zircon and apatite U-Th-He dates of ~14.5–11 Ma (Schultz et al., 2017). Meteoric water has been shown to have percolated into the ductile shear zone associated with the STD, causing (re)crystallization of micas (and titanites) from ~16.7–15 Ma (Gebelin et al., 2017). Titanite data in our study ranges from 19.1 ± 1.6 Ma to 15.2 ± 0.9 Ma (Tables 2, 4; Fig. 7), and therefore overlaps and extends beyond the interpreted timing of metamorphism of the Everest schists at ~20 Ma (Cottle et al., 2015b), and can be interpreted to have (re)crystallization in the presence of fluid during the final stages of ductile movement on the STD. For example, the Rongbuk Monastery titanite samples yield dates from ~16.9 ± 0.6 Ma to 15.6 ± 0.5 Ma, overlapping the final stages of ductile shearing on the STD. In Hermit's gorge, ages increase from 15.2 ± 0.9 Ma (sample ET-16) to 19.1 ± 1.6 Ma (sample R03-36) in the immediate vicinity of the shear zone. In sample ET-16, titanite is associated with clinopyroxene reaction textures, whereas in samples with older titanite ages, R03-36 and 40, titanite is a stable matrix phase. This indicates that titanites in pockets of the Everest schists record older metamorphic conditions and have survived resetting during shearing and fluid flow in the shear zone, possibly due to the patchy nature of fluid flow. Bulk composition and fluid can again be interpreted to play an important role in whether titanite recrystallizes during deformation (i.e. sample ET-16) or whether older generations of titanite are preserved (in the case of samples R03-36 and 40).

5.2.3 Kanchenjunga, eastern Nepal

In the Kachenjunga region of far-eastern Nepal, the GHS is defined by an upper and lower unit, where metamorphic monazite dates progressively decrease down section (Fig. 7). Prograde metamorphism occurs at ~40–25 Ma, followed by melting at ~25 Ma and retrogression between 24 Ma abd 20 Ma in the upper structural levels of the GHS (Ambrose et al., 2015). While in the structurally lower units, prograde metamorphism is interpreted to have occurred ~25–18 Ma and retrograde metamorphism at between ~18 Ma and 13 Ma (Ambrose et al., 2015; Fig. 6a). In the upper levels of the GHS retrograde metamorphism is therefore interpreted to have occurred at the same time as prograde metamorphism in the lower structural levels. This is indicative of progressive accretion of material into the HMC (e.g. Larson et al., 2015). Monazite rims in sample KA044 from Ambrose et al., (2015), located within the structurally lower part of the GHS, grew during melt crystallization >800°C at ~17–16 Ma; these dates overlap, within uncertainty, both the U-Pb (17.4 ± 1.7 Ma) and Zr-in-titanite temperature (814 ± 45°C) from titanite sample 08-57 from the Kachenjunga Himalaya from this study (Fig. 6a). A pronounced Eu anomaly within the trace element pattern of the same sample supports coeval titanite and peritectic feldspar crystallization from melt (Supplementary Material S3). Later titanite growth at 13.7 ± 0.5 Ma (806 ± 44°C) recorded by sample 09-25, from the Kachenjunga area, suggests further (re-)crystallization of titanite on the early decompression path until ~14

Ma (Fig. 6a). Similar trends are seen within other samples where titanite ages are comparable to previously published P-T-t paths from monazite-bearing pelitic samples in nearby Sikkim (Fig. 6b), indicating that titanite within the GHS along-strike grew through peak, to retrograde metamorphic conditions during initial decompression of the GHS. These overlapping ages and temperatures demonstrate that titanite records ages that are very close to peak metamorphism, and support a high (>600°C) closure temperature to Pb diffusion in titanite (Schärer, U. et al., 1984; Zhang and Scharer, 1996; Kohn and Corrie, 2011; Gao et al., 2012; Spencer et al., 2013; Stearns et al., 2015).

5.2.4 Jomolhari, western Bhutan

The Jomolhari dome exposes the high grade metamorphic GHS rocks in far western Bhutan and is bound by the N–S trending Yadong-Gulu graben normal fault and Lingtse fault (Fig. 7). This area is interpreted to have undergone a prolonged metamorphic history between ~38 Ma and 18 Ma (Kellett et al., 2009; Grujic et al., 2011; Regis et al., 2014, 2016; Fig. 6b). Monazite and zircon U-Pb data reveal an early high P phase between ~38 Ma and 36 Ma, followed by up to 15 Ma of prolonged heating and prograde metamorphism up to 800°C between 35 Ma and 29 Ma, and final melt crystallization at 18 Ma (Regis et al., 2014, 2016; Fig. 6b). Monazite in sample DRB1229 records prograde 36 Ma sub-solidus crystallization, which was subsequently rimmed by peritectic monazite at 18 Ma (Fig. 6b). Samples from our study overlap in both age and temperature with the later part of this metamorphic history; titanite cores in sample DRB1233 yield a U-Pb intercept age of 19.6 ± 1.3 Ma and a Zr-in-titanite temperature of 757 ± 40°C, DRB1219 yields an average titanite age of 18.2 ± 2.3 Ma and temperature of 730 ± 38°C. Titanite rims on sample DRB1233 record a further stage of titanite growth at 16.1 ± 0.9 Ma and temperatures of ~779 ± 41°C, potentially during initial decompression (Fig. 6b). Titanite from other samples in the region located in the area of the Yadong-cross structure, yield dates as young as 13 ± 0.5 Ma and temperatures of 716 ± 38°C (sample DRB1213). In this area, simultaneous movement on the STD as well as the Yadong-Gulu graben system and Lingtse fault is thought to have occurred until at least 15–14 Ma (Kellett et al., 2009; Cooper et al., 2015). The titanite dates here could therefore record the final stages of decompression of the GHS rocks due to movement on the Lingtse/Yadong system of normal faults.

5.3 Large-scale trends

5.3.1 Eastward younging in the Himalayan Metamorphic Core

Titanite U-Pb data from our study consistently record ages of ~30–20 Ma throughout the orogen, with dates between ~15 Ma and 12 Ma only seen east of Mt. Everest (Fig. 8a; Table 4). The oldest titanite dates from each transect vary between 28.6 ± 1.7 Ma (Western Nepal) and 17.2 ± 0.7 Ma (Central Bhutan), with no systematic younging trend within these oldest titanite data along-strike (Table 3; Fig. 9). The youngest titanite dates range from 20.5 ± 2.9 Ma (in the Sutlej Valley) to 12.5 ± 0.4 Ma in western Bhutan, and displaying a significant younging trend within the youngest titanite ages in each transect (R^2 = 0.7, Table 4; Fig. 9). The eastward younging trend within the youngest titanite data is supported by the body of previously published monazite and titanite U-Th-Pb data from the HMC (Fig. 8b; Table 5 and references therein) where the youngest recorded ages in each transect decrease towards the east, with the youngest monazite or titanite ages ranging from 17.9 ± 0.1 Ma (Sutlej valley) to 11.5 ± 0.4 Ma (Arunarchal; Table 5); this is similar to the compilation of previously published leucogranite crystallization ages (Fig. 7 and references in Supplementary Table S3). Combined, this dataset shows that Oligocene to early Miocene metamorphic processes have consistently occurred throughout the HMC along-strike, however late Miocene metamorphism has only occurred in the eastern Himalaya. Until now, this trend had not been supported by a single, internally-consistent dataset. The confirmation of this trend by titanite petrochronology, solidifies this approach as a robust method for constraining the timing and temperatures of metamorphic processes elsewhere.

5.3.2 Across strike variations within the HMC

Our dataset reveals that titanite in largely meta-carbonate rocks commonly record a similar T-t path to monazite in interleaved meta-pelitic samples (Fig. 6). The overlap between titanite and monazite datasets highlights the usefulness of titanite for recording the peak to retrograde metamorphic history in rocks, such as calc-silicates, that have traditionally been difficult to estimate P-T-t conditions. This allows for confidence in the interpretation of titanite ages and temperatures yielded from metamorphic rocks. This study therefore demonstrates that titanite petrochronology is a useful tool for providing T-t constraints in other regions, beyond the Himalaya, that lack pelitic assemblages.

When comparing the P-T-t paths and duration of metamorphism recorded between transects, the rocks have largely experienced similar P-T paths, with the exception that the Annapurna Himalaya records a lower temperature history (Fig. 6). There are, however, some discrepancies between the timing of metamorphism between transects. For example, although most of the studied transects were at peak temperature from ~36 Ma to 26 Ma, the rocks were subsequently exhumed at different rates in different transects (Fig. 6). Differences in the timing of exhumation along-strike may be explained by variations in the style, timing and nature of development of underlying structures (e.g. the Lesser Himalayan Duplex) in different transects along-strike (discussed below).

There are variations in the duration of metamorphism recorded by our titanite data along-strike, for example western Nepal (Braden et al., 2017; La Roche et al., 2018) and the Kachenjunga region of eastern Nepal and Sikkim (Rubatto et al., 2013; Ambrose et al., 2015) record a longer duration of metamorphism than the Sutlej Valley and central Bhutan (Table 5). This ‘pinching and swelling’ of the metamorphic history can clearly be shown in the compilation of data in Fig. 8b. Although this overall pattern could be an artifact of sample bias, if real, it is likely to reflect differences in the mechanisms responsible for the addition, extrusion and exhumation of the rocks within the HMC along-strike (discussed below).

When titanite dates from our study are plotted with respect to their location along-strike and colour-contoured by the estimated structural thickness of the HMC in that area (Fig. 10), a general trend is evident where transects with a thicker HMC (up to ~35 km structural thickness), yield the largest differences in Zr-in-titanite temperatures, with temperatures varying up to 128°C between grains in one transect (Table 4). Areas with a thicker HMC also tend to yield some of the youngest titanite U-Pb dates, for example, sample SK12-119 from the Sikkim Himalaya, where the GHS is ~30 km thick, yields a titanite age of 14.8 ± 0.5 Ma (Table 4).

5.3.3 Tectonometamorphic evolution of the HMC

Our dataset reveal (1) broad eastward, along-strike younging within the timing of final crystallization of titanite, (2) differences in the duration of metamorphism within the HMC along strike, and (3) correlation between the thickness of the GHS and the temperatures and timing of metamorphism. It is beyond the scope of this manuscript to pose a thermomechanical model to explain these trends, but such observations raise some important questions about the causal relationships between different tectono-metamorphic processes in the Himalaya.

a. The broad along-strike younging seen in the timing of metamorphism in the HMC may be explained by the overall asymmetry of the timing and amount of shortening during the India-Asia collision (Molnar and Tapponier, 1975; Klootwijk et al., 1985; Treloar and Coward, 1991; Banerjee et al., 2008; Molar and Stock, 2009; Replumaz et al., 2010). However, there remain unanswered questions about why consistent Oligocene to early Miocene metamorphic dates are recorded along the length of the HMC, with mid to late Miocene ages only in the east. Potential models to explain this could involve variations in processes in the lithospheric mantle (Gahalaut and Kundu, 2012; Hammer et al., 2013; Chen et al., 2015; Hetényi et al., 2016; Webb et al., 2017) or due to the geometry and evolution of the orogen-controlling structures (see 2).

b. The location and migration of ramps on the MHT are key factors for controlling the temporal and thermal evolution of the HMC and for controlling the location of ductile duplexing and accretion of rock into the HMC through time (e.g. Larson et al., 2015; Mercier et al., 2017)., and can therefore explain the disparities in the timing, duration and temperature of metamorphism in the HMC between transects. When small ramps on the MHT are located directly beneath the Main Boundary Thrust, such as in western Nepal (Robert et al., 2011), movement is likely to be dominated by the formation of a thick duplex of material in the Lesser Himalayan and therefore a thinner GHS material (Mercier et al., 2017; Figure 11a). Where ramps are located towards the hinterland (such as in central-eastern Nepal; Jouanne et al., 2004), the basal detachment is at a more mature stage in the ramp accretion cycle and thus there has been more time for material to accrete into the thrust system (Mercier et al., 2017; Figure 11b).

A conceptual model can be developed from our data, where a thicker GHS, such as eastern Nepal and the Sikkim Himalaya (Ambrose et al., 2015; Mottram et al., 2015a, respectively), is formed in the eastern Himalaya due to multiple footwall accretion events and/or out-of-sequence thrusts (i.e. Montimoli et al., 2015) adding material to the HMC throughout the Miocene (e.g. Larson et al., 2015). A hinterland-located ramp on the basal decollement (i.e. the MHT) throughout the Miocene would have resulted in the prolonged ductile accretion of material into the GHS (Fig. 11b). This is supported by data from this study where transects with a structurally thicker GHS such as in eastern Nepal, also yield the largest range of titanite ages, which spread between ~26 Ma and 12.5 Ma (Fig. 10). Disparities in the timing, duration and temperature of metamorphism in the HMC between transects may therefore be explained by differences in the geometry of the orogen-scale decollement, however further work is needed to fully understand the 3D evolution of the MHT through time.

c. Differences in the accretion, duplexing and exhumation history, largely controlled through the formation of the Lesser Himalayan Duplexes (e.g. Robinson and McQuarrie, 2012), are likely very important processes for controlling differential exposure of varying structural levels of the HMC. Through this process, material that was accreted into the GHS more recently is brought up to the surface, thus exposing samples with younger metamorphic ages in thicker exposures of the HMC (Figs. 10,11; Larson et al., 2015, 2017). Differences in the accretion, duplexing and exhumation history along-strike may help explain the differences in timing of exhumation between transects (e,g, Figs. 6, 8b). Moreover, the eastward increase in rainfall rates and specific stream power (e.g. Duncan et al., 2003; Hirshmiller et al., 2014), potentially forced by tectonically-driven orographic controls, could be an important compounding factor for focusing preferential erosion and thus exposing the thicker, younger HMC in the east of the orogen.

d. The presence of pre-existing basement structures within the Indian crust (e.g. Godin et al., 2018) could potentially provide a mechanism for explaining differences in the location of ramps on the MHT along-strike. For example, there is a major shift in the duration of metamorphism between the Sutlej Valley (~11 Ma) and the Karnali Klippe (~44 Ma), which are separated by the Delhi-Hariwar ridge. The Faizabad ridge separates western from central Nepal and the Mungo-Saharsa ridge separates eastern Nepal and Sikkim from Bhutan (Godin et al., 2018). These structures therefore may have had a major influence on the along-strike geometry of the MHT and thus the accretionary history of the HMC.

6. CONCLUSIONS

We present a 'campaign-style' petrochronological study of titanite U-Th-Pb-REE-Zr data from 47 calc-silicate samples from >2000 km along-strike distance along the GHS crystalline core of the Himalaya. The results indicate that titanite U-Pb ages commonly represent crystallization rather than cooling ages and can therefore be used to understand the timing, duration and temperature conditions of metamorphic processes. When compared as a whole, all titanite crystallised at temperatures of 620–810°C. The oldest titanite U-Pb dates are consistently between ~30 Ma and 20 Ma along the entire length of the studied area, with an eastward-younging trend in the youngest titanite dates, which are as young as ~12 Ma east of Mt. Everest. The titanite data presented here are interpreted to indicate that lateral variations in the geometry of the basal decollement play an important role in controlling the amount and timing of ductile accretion into the HMC at depth, leading to heterogeneities in the duration and minimum timing of metamorphism between transects. A transition to duplexing within the underlying Lesser Himalayan rocks towards the foreland, coupled with erosion at the surface led to differential exposure of a younger and thicker GHS in the east of the orogen. This study represents the only internally-consistent orogen-scale study of its type in the Himalaya and demonstrates the potential for 'campaign-style' petrochronology for revealing large-scale lateral variations in the timing of deformation in collisional orogens.

ACKNOWLEDGEMENTS

This project would not have been possible without the donation of samples from Tom Argles, Rodolfo Carosi, Jen Chambers, Frances Cooper, Stacia Gordon, Chiara Groppo, Djordje Grujic, Tom Hopkinson, Nigel Harris, Matt Kohn, Rick Law, Aaron Martin, Andy Parsons, Daniele Regis, Delores Robinson, Clare Warren and Alex Webb. This study was funded by a UK-US all-discipline Fulbright commission scholarship awarded to C.Mottram and UCSB funds to J.Cottle. Thanks to Gareth Seward for help with SEM and EPMA analyses and to Kyle Larson and Dawn Kellett for comments on the manuscript. Rick Law, Chris Clark and an anonymous reviewer are thanked for reviews on an earlier version of this manuscript. Extensive editor comments and reviews from Kyle Larson, Aaron Martin and an anonymous reviewer considerably improved this version of the manuscript.

REFERENCES CITED

Adams, B.A., Whipple, K.X., Hodges, K. V., and Heimsath, A.M., 2016, In situ development of high-elevation, low-relief landscapes via duplex deformation in the Eastern Himalayan hinterland, Bhutan: Journal of Geophysical Research: Earth Surface, v. 121, p. 294–319, doi: 10.1002/2015JF003508.

Aleinikoff, J. N., Wintsch, R. P., Fanning, C. M., & Dorais, M. J., 2002. U–Pb geochronology of zircon and polygenetic titanite from the Glastonbury Complex, Connecticut, USA: an integrated SEM, EMPA, TIMS, and SHRIMP study. *Chemical Geology*, *188*(1-2), 125-147.

Ambrose, T.K., Larson, K.P., Guilmette, C., Cottle, J.M., Buckingham, H., and Rai, S., 2015, Lateral extrusion, underplating, and out-of-sequence thrusting within the Himalayan metamorphic core, Kanchenjunga, Nepal: Lithosphere, p. 1–25, doi: 10.1130/L437.1.

Banerjee, P., Burgmann, R., Nagarajan, B., and Apel, E., 2008, Intraplate deformation of the Indian subcontinent: Geophysical Research Letters, v. 35, p. 1–5, doi: 10.1029/2008GL035468.

Beaumont, C., Jamieson, R. A., Nguyen, M. H., & Lee, B., 2001. Himalayan tectonics explained by extrusion of a low-viscosity crustal channel coupled to focused surface denudation. *Nature*, *414*(6865), 738.

Berger, A., Jouanne, F., Hassani, R., and Mugnier, J.L., 2004, Modelling the spatial distribution of present-day deformation in Nepal: How cylindrical is the Main Himalayan Thrust in Nepal? Geophysical Journal International, v. 156, p. 94–114, doi: 10.1111/j.1365-246X.2004.02038.x.

Bookhagen, B., and Burbank, D.W., 2010, Toward a complete Himalayan hydrological budget: Spatiotemporal distribution of snowmelt and rainfall and their impact on river discharge: Journal of Geophysical Research: Earth Surface, v. 115, p. 1–25, doi: 10.1029/2009JF001426.

Braden, Z., Godin, L., & Cottle, J. M., 2017. Segmentation and rejuvenation of the Greater Himalayan sequence in western Nepal revealed by in situ U–Th/Pb monazite petrochronology. *Lithos*, *284*, 751-765.

Burgess, P.W., Yin, A., Dubey, C.S., Shen, Z.K., and Kelty, T.K., 2012, Holocene shortening across the main frontal thrust zone in the eastern Himalaya: Earth and Planetary Science Letters, v. 357–358, p. 152–167, doi: 10.1016/j.epsl.2012.09.040.

Catlos, E. J., Harrison, T. M., Kohn, M. J., Grove, M., Ryerson, F. J., Manning, C. E., & Upreti, B. N., 2001. Geochronologic and thermobarometric constraints on the evolution of the Main Central Thrust, central Nepal Himalaya. *Journal of Geophysical Research: Solid Earth*, *106*(B8), 16177-16204.

Carosi, R., Montomoli, C., & Visonà, D., 2007. A structural transect in the Lower Dolpo: Insights on the tectonic evolution of Western Nepal. *Journal of Asian Earth Sciences*, *29*(2-3), 407-423.

Carosi, R., Montomoli, C., Rubatto, D., & Visonà, D., 2010. Late Oligocene high-temperature shear zones in the core of the Higher Himalayan Crystallines (Lower Dolpo, western Nepal). *Tectonics*, *29*(4).

Carosi, R., Montomoli, C., Langone, A., Turina, A., Cesare, B., Iaccarino, S & Ronchi, A., 2015. Eocene partial melting recorded in peritectic garnets from kyanite-gneiss, Greater Himalayan Sequence, central Nepal. *Geological Society, London, Special Publications*, *412*(1), 111-129.

Carosi, R., Montomoli, C., Iaccarino, S., Massonne, H. J., Rubatto, D., Langone, A., ... & Visonà, D., 2016. Middle to late Eocene exhumation of the Greater Himalayan Sequence in the Central Himalayas: Progressive accretion from the Indian plate. *Bulletin*, *128*(11-12), 1571-1592.

Carosi, R., Montomoli, C., & Iaccarino, S., 2017. 20 years of geological mapping of the metamorphic core across Central and Eastern Himalayas. *Earth-Science Reviews, 177, 124-138*.

Chambers, J. A., Argles, T. W., Horstwood, M. S. A., Harris, N. B. W., Parrish, R. R., & Ahmad, T., 2008. Tectonic implications of Palaeoproterozoic anatexis and Late Miocene metamorphism in the Lesser Himalayan Sequence, Sutlej Valley, NW India. *Journal of the Geological Society*, *165*(3), 725-737.

Chen, B., Liu, J., Chen, C., Du, J., and Sun, Y., 2015, Elastic thickness of the Himalayan–Tibetan orogen estimated from the fan wavelet coherence method, and its implications for lithospheric structure: Earth and Planetary Science Letters, v. 409, p. 1–14, doi: 10.1016/j.epsl.2014.10.039.

Cherniak, D.J., 1993, Lead diffusion in titanite and preliminary results on the effects of radiation damage on Pb transport: Chemical Geology, v. 110, p. 177–194, doi: 10.1016/0009-2541(93)90253-F.

Cherniak, D. J., 2006. Zr diffusion in titanite. *Contributions to Mineralogy and Petrology*, *152*(5), 639-647.

Cooper, F. J., Adams, B. A., Edwards, C. S., & Hodges, K. V., 2012. Large normal-sense displacement on the South Tibetan fault system in the eastern Himalaya. *Geology*, *40*(11), 971-974.

Cooper, F. J., Hodges, K. V., Parrish, R. R., Roberts, N. M. W., & Horstwood, M. S. A., 2015. Synchronous N-S and E-W extension at the Tibet-to-Himalaya transition in NW Bhutan. *Tectonics*, *34*(7), 1375-1395.

Corrie, S. L., & Kohn, M. J., 2011. Metamorphic history of the central Himalaya, Annapurna region, Nepal, and implications for tectonic models. *Bulletin*, *123*(9-10), 1863-1879.

Cottle, J.M., Larson, K.P., and Kellett, D.A., 2015a, How does the mid-crust accommodate deformation in large, hot collisional orogens? A review of recent research in the Himalayan orogen: Journal of Structural Geology, v. 78, p. 119–133, doi: 10.1016/j.jsg.2015.06.008.

Cottle, J. M., Searle, M. P., Jessup, M. J., Crowley, J. L., & Law, R. D., 2015b. Rongbuk re-visited: Geochronology of leucogranites in the footwall of the South Tibetan detachment system, Everest region, southern Tibet. *Lithos*, *227*, 94-106.

Coutand, I., Whipp, D.M., Grujic, D., Bernet, M., Fellin, M.G., Bookhagen, B., Landry, K.R., Ghalley, S.K., and Duncan, C., 2014, Geometry and kinematics of the Main Himalayan Thrust and Neogene crustal exhumation in the Bhutanese Himalaya derived from inversion of multithermochronologic data: Journal of Geophysical Research: Solid Earth, v. 119, p. 1446–1481, doi: 10.1002/2013JB010891.

Daniel, C. G., Hollister, L. S., Parrish, R. T., & Grujic, D., 2003. Exhumation of the Main Central Thrust from lower crustal depths, eastern Bhutan Himalaya. *Journal of Metamorphic Geology*, *21*(4), 317-334.

Dasgupta, S., Ganguly, J., & Neogi, S., 2004. Inverted metamorphic sequence in the Sikkim Himalayas: crystallization history, P–T gradient and implications. *Journal of Metamorphic Geology*, *22*(5), 395-412.

Davis, D., Suppe, J., & Dahlen, F. A., 1983. Mechanics of fold-and-thrust belts and accretionary wedges. *Journal of Geophysical Research: Solid Earth*, *88*(B2), 1153-1172.

DeCelles, P. G., Gehrels, G. E., Quade, J., & Ojha, T. P., 1998. Eocene-early Miocene foreland basin development and the history of Himalayan thrusting, western and central Nepal. *Tectonics*, *17*(5), 741-765.

DeCelles, P. G., Carrapa, B., Gehrels, G. E., Chakraborty, T., & Ghosh, P., 2016. Along-strike continuity of structure, stratigraphy, and kinematic history in the Himalayan thrust belt: The view from Northeastern India. *Tectonics*, *35*(12), 2995-3027.

Duncan, C., Masek, J., and Fielding, E., 2003, How steep are the Himalaya? Characteristics and implications of along-strike topographic variations: Geology, v. 31, p. 75–78, doi: 10.1130/0091-7613(2003)031<0075:HSATHC>2.0.CO;2.

Engi, M., Lanari, P., & Kohn, M. J., 2017. Significant ages—An introduction to petrochronology. *Reviews in mineralogy and geochemistry*, *83*(1), 1-12.

From, R., Larson, K., & Cottle, J. M., 2014. Metamorphism and geochronology of the exhumed Himalayan midcrust, Likhu Khola region, east-central Nepal: Recognition of a tectonometamorphic discontinuity. *Lithosphere*, *6*(5), 361-376.

Frost, B. R., Chamberlain, K. R., & Schumacher, J. C., 2001. Sphene (titanite): phase relations and role as a geochronometer. *Chemical geology*, *172*(1-2), 131-148.

Gahalaut, V.K., and Kundu, B., 2012, Possible influence of subducting ridges on the Himalayan arc and on the ruptures of great and major Himalayan earthquakes: Gondwana Research, v. 21, p. 1080–1088, doi: 10.1016/j.gr.2011.07.021.

Gao, X. Y., Zheng, Y. F., Chen, Y. X., & Guo, J., 2012. Geochemical and U–Pb age constraints on the occurrence of polygenetic titanites in UHP metagranite in the Dabie orogen. *Lithos*, *136*, 93-108.

Garber, J. M., Hacker, B. R., Kylander-Clark, A. R. C., Stearns, M., & Seward, G., 2017. Controls on Trace Element Uptake in Metamorphic Titanite: Implications for Petrochronology. *Journal of Petrology*, *58*(6), 1031-1057.

Gibson, R., Godin, L., Kellett, D.A., Cottle, J.M., and Archibald, D., 2016, Diachronous deformation along the base of the Himalayan metamorphic core, west-central Nepal: GSA Bulletin, v. 128, p. 860–878, doi: 10.1130/B31328.1.

Godin, L., & Harris, L. B., 2014. Tracking basement cross-strike discontinuities in the Indian crust beneath the Himalayan orogen using gravity data–relationship to upper crustal faults. *Geophysical Journal International*, *198*(1), 198-215.

Godin, L., Parrish, R. R., Brown, R. L., & Hodges, K. V., 2001. Crustal thickening leading to exhumation of the Himalayan metamorphic core of central Nepal: Insight from U-Pb geochronology and 40Ar/39Ar thermochronology. *Tectonics*, *20*(5), 729-747.

Godin, L., La Roche, R. S., Waffle, L., & Harris, L. B., 2018. Influence of inherited Indian basement faults on the evolution of the Himalayan Orogen. *Geological Society, London, Special Publications*, *481*, SP481-4.

Goscombe, B., Gray, D., & Hand, M., 2006. Crustal architecture of the Himalayan metamorphic front in eastern Nepal. *Gondwana Research*, *10*(3-4), 232-255.

Goscombe, B., Gray, D., & Foster, D. A., 2018. Metamorphic response to collision in the Central Himalayan Orogen. *Gondwana Research*.

Groppo, C., Rolfo, F., & Lombardo, B., 2009. P–T evolution across the Main Central Thrust Zone (Eastern Nepal): hidden discontinuities revealed by petrology. *Journal of Petrology*, *50*(6), 1149-1180.

Groppo, C., Rolfo, F., Castelli, D., & Connolly, J. A., 2013a. Metamorphic CO 2 production from calc-silicate rocks via garnet-forming reactions in the CFAS–H 2 O–CO 2 system. *Contributions to mineralogy and petrology*, *166*(6), 1655-1675.

Groppo, C., Rolfo, F., & Mosca, P., 2013b. The cordierite-bearing anatectic rocks of the higher Himalayan crystallines (eastern Nepal): low-pressure anatexis, melt productivity, melt loss and the preservation of cordierite. *Journal of Metamorphic Geology*, *31*(2), 187-204.

Groppo, C., Rolfo, F., Castelli, D., and Mosca, P., 2017, Metamorphic CO2 production in collisional orogens: Petrological constraints from phase diagram modelling of Himalayan, scapolite-bearing, calc-silicate rocks in the NKC(F)MAS(T)-HC system: Journal of Petrology, v. 58, p. 53–83, http://dx.doi.org/10.1093/petrology/egx005.

Grujic, D., Casey, M., Davidson, C., Hollister, L. S., Kündig, R., Pavlis, T., & Schmid, S., 1996. Ductile extrusion of the Higher Himalayan Crystalline in Bhutan: evidence from quartz microfabrics. *Tectonophysics*, *260*(1-3), 21-43.

Grujic, D., Warren, C. J., & Wooden, J. L., 2011. Rapid synconvergent exhumation of Miocene-aged lower orogenic crust in the eastern Himalaya. *Lithosphere*, *3*(5), 346-366.

Guillot, S., Cosca, M., Allemand, P., and Le Fort, P., 1999, Contrasting metamorphic and geochronologic evolution along the Himalayan belt, in Macfarlane, A., Sorkhabi, R.B., and Quade, J., eds., Himalaya and Tibet: Mountain Roots to Mountain Tops: Boulder, Colorado, Geological Society of America Special Paper 328, 117-128.

Hammer, P., Berthet, T., Hetényi, G., Cattin, R., Drukpa, D., Chophel, J., Lechmann, S., Moigne, N. Le, Champollion, C., and Doerflinger, E., 2013, Flexure of the India plate underneath the Bhutan Himalaya: Geophysical Research Letters, v. 40, p. 4225–4230, doi: 10.1002/grl.50793.

Harlov, D., Tropper, P., Seifert, W., Nijland, T., & Förster, H. J., 2006. Formation of Al-rich titanite (CaTiSiO4O–CaAlSiO4OH) reaction rims on ilmenite in metamorphic rocks as a function of fH2O and fO2. *Lithos*, *88*(1-4), 72-84.

Harvey, J.E., Burbank, D.W., and Bookhagen, B., 2015, Along-strike changes in Himalayan thrust geometry: Topographic and tectonic discontinuities in western Nepal: Lithosphere, v. 7, p. 511–518, doi: 10.1130/L444.1.

Hauck, M. L., Nelson, K. D., Brown, L. D., Zhao, W., & Ross, A. R. 1998. Crustal structure of the Himalayan orogen at~ 90 east longitude from Project INDEPTH deep reflection profiles. *Tectonics*, *17*(4), 481-500.

Hayden, L.A., Watson, E.B., and Wark, D.A., 2008, A thermobarometer for sphene (titanite): Contributions to Mineralogy and Petrology, v. 155, p. 529–540, doi: 10.1007/s00410-007-0256-y.

He, D., Webb, A. A. G., Larson, K. P., Martin, A. J., & Schmitt, A. K., 2015. Extrusion vs. duplexing models of Himalayan mountain building 3: Duplexing dominates from the Oligocene to Present. *International Geology Review*, *57*(1), 1-27.

Hermann, J., Rubatto, D., Korsakov, A., & Shatsky, V. S., 2001. Multiple zircon growth during fast exhumation of diamondiferous, deeply subducted continental crust (Kokchetav Massif, Kazakhstan). *Contributions to Mineralogy and Petrology*, *141*(1), 66-82.

Hetényi, G., Cattin, R., Berthet, T., Le Moigne, N., Chophel, J., Lechmann, S., Hammer, P., Drukpa, D., Sapkota, S.N., Gautier, S., and Thinley, K., 2016, Segmentation of the Himalayas as revealed by arc-parallel gravity anomalies: Scientific Reports, v. 6, p. 33866, doi: 10.1038/srep33866.

Hirschmiller, J., Grujic, D., Bookhagen, B., Coutand, I., Huyghe, P., Mugnier, J.-L., and Ojha, T., 2014, What controls the growth of the Himalayan foreland fold-and-thrust belt? Geology, v. 42, p. 247–250, http://10.0.4.106/G35057.1.

Hodges, K. V, 2000, Tectonics of the Himalaya and southern Tibet from two perspectives: GSA Bulletin, v. 112, p. 324–350, http://dx.doi.org/10.1130/0016-7606(2000)112%3C324:TOTHAS%3E2.0.CO.

Iaccarino, S., Montomoli, C., Carosi, R., Massonne, H. J., Langone, A., & Visonà, D., 2015. Pressure–temperature–time–deformation path of kyanite-bearing migmatitic paragneiss in the Kali Gandaki valley (Central Nepal): Investigation of Late Eocene–Early Oligocene melting processes. *Lithos*, *231*, 103-121.

Inger, S., & Harris, N., 1993. Geochemical constraints on leucogranite magmatism in the Langtang Valley, Nepal Himalaya. *Journal of Petrology*, *34*(2), 345-368.

Jamieson, R. A., & Beaumont, C., 2013. On the origin of orogens. *Bulletin*, *125*(11-12), 1671-1702.

Jamieson, R. A., Beaumont, C., Nguyen, M. H., & Grujic, D. 2006. Provenance of the Greater Himalayan Sequence and associated rocks: predictions of channel flow models. *Geological Society, London, Special Publications*, *268*(1), 165-182.

Jessup, M. J., Cottle, J. M., Searle, M. P., Law, R. D., Newell, D. L., Tracy, R. J., & Waters, D. J., 2008. P–T–t–D paths of Everest Series schist, Nepal. *Journal of Metamorphic Geology*, *26*(7), 717-739.

Jouanne, F., Mugnier, J.L., Gamond, J.F., Le Fort, P., Pandey, M.R., Bollinger, L., Flouzat, M., and Avouac, J.P., 2004, Current shortening across the Himalayas of Nepal: Geophysical Journal International, v. 157, p. 1–14, http://dx.doi.org/10.1111/j.1365-246X.2004.02180.x.

Kellett, D. A., & Grujic, D., 2012. New insight into the South Tibetan detachment system: Not a single progressive deformation. *Tectonics*, *31*(2).

Kellett, D. A., Grujic, D., Warren, C., Cottle, J., Jamieson, R., & Tenzin, T., 2010. Metamorphic history of a syn-convergent orogen-parallel detachment: The South Tibetan detachment system, Bhutan Himalaya. *Journal of Metamorphic Geology*, *28*(8), 785-808.

Kellett, D. A., Grujic, D., Coutand, I., Cottle, J., & Mukul, M., 2013. The South Tibetan detachment system facilitates ultra rapid cooling of granulite-facies rocks in Sikkim Himalaya. *Tectonics*, *32*(2), 252-270.

Klootwijk, C.T., Conaghan, P.J., and Powell, C.M., 1985, The Himalayan Arc: large-scale continental subduction, oroclinal bending and back-arc spreading: Earth and Planetary Science Letters, v. 75, p. 167–183, doi: 10.1016/0012-821X(85)90099-8.

Kohn, M. J., 2008. PTt data from central Nepal support critical taper and repudiate large-scale channel flow of the Greater Himalayan Sequence. *Geological Society of America Bulletin*, *120*(3-4), 259-273.

Kohn, M. J., Wieland, M. S., Parkinson, C. D., & Upreti, B. N. 2005. Five generations of monazite in Langtang gneisses: implications for chronology of the Himalayan metamorphic core. *Journal of Metamorphic Geology*, *23*(5), 399-406.

Kohn, M.J., 2014, Himalayan metamorphism and its tectonic implications: v. 42, 381-419 p., doi: 10.1146/annurev-earth-060313-055005.

Kohn, M. J., 2017. Titanite petrochronology. *Reviews in Mineralogy and Geochemistry*, *83*(1), 419-441.

Kohn, M. J., & Corrie, S. L., 2011. Preserved Zr-temperatures and U–Pb ages in high-grade metamorphic titanite: evidence for a static hot channel in the Himalayan orogen. *Earth and Planetary Science Letters*, *311*(1-2), 136-143.

Kohn, M. J., Wieland, M. S., Parkinson, C. D., & Upreti, B. N., 2004. Miocene faulting at plate tectonic velocity in the Himalaya of central Nepal. *Earth and Planetary Science Letters*, *228*(3-4), 299-310.

Kylander-Clark, A. R. C., Hacker, B. R., & Mattinson, J. M, 2008. Slow exhumation of UHP terranes: titanite and rutile ages of the Western Gneiss Region, Norway. *Earth and Planetary Science Letters*, *272*(3-4), 531-540.

Kylander-Clark, A. R., Hacker, B. R., & Cottle, J. M., 2013. Laser-ablation split-stream ICP petrochronology. *Chemical Geology*, *345*, 99-112.

La Roche, R. S., Godin, L., Cottle, J. M., & Kellett, D. A., 2018. Preservation of the early evolution of the Himalayan middle crust in foreland klippen: insights from the Karnali klippe, west Nepal. *Tectonics*.

Langille, J. M., Jessup, M. J., Cottle, J. M., Lederer, G., & Ahmad, T., 2012. Timing of metamorphism, melting and exhumation of the Leo Pargil dome, northwest India. *Journal of Metamorphic Geology*, *30*(8), 769-791.

Larson, K. P., & Cottle, J. M., 2014. Midcrustal discontinuities and the assembly of the Himalayan midcrust. *Tectonics*, *33*(5), 718-740.

Larson, K. P., & Cottle, J. M., 2015. Initiation of crustal shortening in the Himalaya. *Terra Nova*, *27*(3), 169-174.

Larson, K.P., Ambrose, T.K., Webb, A.G., Cottle, J.M., and Shrestha, S., 2015, Reconciling Himalayan midcrustal discontinuities: The Main Central thrust system: Earth and Planetary Science Letters, v. 429, p. 139–146, doi: 10.1016/j.epsl.2015.07.070.

Larson, K.P., Camacho, A., Cottle, J.M., Coutand, I., Buckingham, H.M., Ambrose, T.K., and Rai, S.M., 2017, Cooling, exhumation, and kinematics of the Kanchenjunga Himal, far east Nepal: Tectonics, p. 1–16, doi: 10.1002/2017TC004496.

Larson, K. P., Ali, A., Shrestha, S., Soret, M., Cottle, J. M., & Ahmad, R. 2018. Timing of metamorphism and deformation in the Swat valley, northern Pakistan: insight into garnet-monazite HREE partitioning. *Geoscience Frontiers*.

Lederer, G. W., Cottle, J. M., Jessup, M. J., Langille, J. M., & Ahmad, T., 2013. Timescales of partial melting in the Himalayan middle crust: insight from the Leo Pargil dome, northwest India. *Contributions to Mineralogy and Petrology*, *166*(5), 1415-1441.

Long, S., McQuarrie, N., Tobgay, T., and Grujic, D., 2011, Geometry and crustal shortening of the Himalayan fold-thrust belt, eastern and central Bhutan: Bulletin of the Geological Society of America, v. 123, p. 1427–1447, doi: 10.1130/B30306.1.

Lucassen, F. and Becchio, R. 2003, Timing of high-grade metamorphism: Early Palaeozoic U–Pb formation ages of titanite indicate long-standing high-*T* conditions at the western margin of Gondwana (Argentina, 26–29°S). Journal of Metamorphic Geology, 21: 649-662. doi:10.1046/j.1525-1314.2003.00471.x

Macfarlane, A. M., 1993. Chronology of tectonic events in the crystalline core of the Himalaya, Langtang National Park, central Nepal. *Tectonics*, *12*(4), 1004-1025.

Martin, A. J., Copeland, P., & Benowitz, J. A., 2015. Muscovite 40Ar/39Ar ages help reveal the Neogene tectonic evolution of the southern Annapurna Range, central Nepal. *Geological Society, London, Special Publications*, *412*(1), 199-220.

Martin, A. J. 2017a. A review of Himalayan stratigraphy, magmatism, and structure. *Gondwana Research*, *49*, 42-80.

Martin, A. J., 2017b. A review of definitions of the Himalayan Main Central Thrust. *International Journal of Earth Sciences*, *106*(6), 2131-2145.

Martin, A. J., Ganguly, J., & DeCelles, P. G., 2010. Metamorphism of Greater and Lesser Himalayan rocks exposed in the Modi Khola valley, central Nepal. *Contributions to Mineralogy and Petrology*, *159*(2), 203.

Mathavan, V., & Fernando, G. W. A. R., 2001. Reactions and textures in grossular–wollastonite–scapolite calc–silicate granulites from Maligawila, Sri Lanka: evidence for high-temperature isobaric cooling in the meta-sediments of the Highland Complex. *Lithos*, *59*(4), 217-232.

Mercier, J., Braun, J., and van der Beek, P., 2017, Do along-strike tectonic variations in the Nepal Himalaya reflect different stages in the accretion cycle? Insights from numerical modeling: Earth and Planetary Science Letters, v. 472, p. 299–308, doi: 10.1016/j.epsl.2017.04.041.

Molnar, P., and Stock, J.M., 2009, Slowing of India's convergence with Eurasia since 20 Ma and its implications for Tibetan mantle dynamics: Tectonics, v. 28, p. 1–11, doi: 10.1029/2008TC002271.

Molnar, P., and Tapponnier, P., 1975, Cenozoic tectonics of Asia : Effects of a continental collision: Science, v. 189, p. 419–426, doi: 10.1126/science.189.4201.419.

Montomoli, C., Iaccarino, S., Carosi, R., Langone, A., & Visonà, D., 2013. Tectonometamorphic discontinuities within the Greater Himalayan Sequence in Western Nepal (Central Himalaya): insights on the exhumation of crystalline rocks. *Tectonophysics*, *608*, 1349-1370.

Montomoli, C., Carosi, R., & Iaccarino, S., 2015. Tectonometamorphic discontinuities in the Greater Himalayan Sequence: a local or a regional feature?. *Geological Society, London, Special Publications*, *412*(1), 25-41.

Mottram, C.M., Parrish, R.R., Regis, D., Warren, C.J., Argles, T.W., Harris, N.B.W., and Roberts, N.M.W., 2015a, Using U-Th-Pb petrochronology to determine rates of ductile thrusting: Time windows into the Main Central Thrust, Sikkim Himalaya: Tectonics, v. 34, p. 1355–1374, doi: 10.1002/2014TC003743.

Mottram, C. M., Warren, C. J., Halton, A. M., Kelley, S. P., & Harris, N. B., 2015b. Argon behaviour in an inverted Barrovian sequence, Sikkim Himalaya: the consequences of temperature and timescale on 40Ar/39Ar mica geochronology. *Lithos*, *238*, 37-51.

Mottram, C.M., Warren, C.J., Regis, D., Roberts, N.M.W., Harris, N.B.W., Argles, T.W., and Parrish, R.R., 2014, Developing an inverted barrovian sequence; insights from monazite petrochronology: Earth and Planetary Science Letters, v. 403, p. 418–431, doi: 10.1016/j.epsl.2014.07.006.

Mottram, C. M., Warren, C. J., Halton, A. M., Kelley, S. P., & Harris, N. B., 2015. Argon behaviour in an inverted Barrovian sequence, Sikkim Himalaya: the consequences of temperature and timescale on 40Ar/39Ar mica geochronology. *Lithos*, *238*, 37-51.

Najman, Y., Appel, E., Boudagher-Fadel, M., Bown, P., Carter, A., Garzanti, E., Godin, L., Han, J., Liebke, U., Oliver, G., Parrish, R., and Vezzoli, G., 2010, Timing of India-Asia collision: Geological, biostratigraphic, and palaeomagnetic constraints: Journal of Geophysical Research, v. 115, p. B12416, doi: 10.1029/2010JB007673.

Parsons, A. J., Law, R. D., Searle, M. P., Phillips, R. J., & Lloyd, G. E., 2016a. Geology of the Dhaulagiri-Annapurna-Manaslu Himalaya, Western Region, Nepal. 1: 200,000. *Journal of Maps*, *12*(1), 100-110.

Parsons, A. J., Phillips, R. J., Lloyd, G. E., Law, R. D., Searle, M. P., & Walshaw, R. D., 2016b. Mid-crustal deformation of the Annapurna-Dhaulagiri Himalaya, central Nepal: An atypical example of channel flow during the Himalayan orogeny. *Geosphere*, *12*(3), 985-1015.

Pidgeon, R. T., Bosch, D., & Bruguier, O., 1996. Inherited zircon and titanite U□ Pb systems in an Archaean syenite from southwestern Australia: implications for U□ Pb stability of titanite. *Earth and Planetary Science Letters*, *141*(1-4), 187-198.

Regis, D., Warren, C. J., Young, D., & Roberts, N. M., 2014. Tectono-metamorphic evolution of the Jomolhari massif: Variations in timing of syn-collisional metamorphism across western Bhutan. *Lithos*, *190*, 449-466.

Regis, D., Warren, C. J., Mottram, C. M., & Roberts, N. M. W., 2016. Using monazite and zircon petrochronology to constrain the P–T–t evolution of the middle crust in the Bhutan Himalaya. *Journal of Metamorphic Geology*, *34*(6), 617-639.

Replumaz, A., Negredo, A.M., Villaseñor, A., and Guillot, S., 2010, Indian continental subduction and slab break-off during Tertiary collision: Terra Nova, v. 22, p. 290–296, doi: 10.1111/j.1365-3121.2010.00945.x.

Robert, X., Van Der Beek, P., Braun, J., Perry, C., and Mugnier, J.L., 2011, Control of detachment geometry on lateral variations in exhumation rates in the Himalaya: Insights from low-temperature thermochronology and numerical modeling: Journal of Geophysical Research: Solid Earth, v. 116, p. 1–22, doi: 10.1029/2010JB007893.

Robinson, D. M., & McQuarrie, N., 2012. Pulsed deformation and variable slip rates within the central Himalayan thrust belt. *Lithosphere*, *4*(5), 449-464.

Robinson, D. M., DeCelles, P. G., & Copeland, P., 2006. Tectonic evolution of the Himalayan thrust belt in western Nepal: Implications for channel flow models. *Geological Society of America Bulletin*, *118*(7-8), 865-885.

Rolfo, F., Groppo, C., and Mosca, P., 2017, Metamorphic CO2 production in calc-silicate rocks from the eastern Himalaya: Italian Journal of Geosciences, v. 136, p. 28–38, doi: 10.3301/IJG.2015.36.

Rubatto, D., & Hermann, J., 2001. Exhumation as fast as subduction?. *Geology*, *29*(1), 3-6.

Rubatto, D., Chakraborty, S., & Dasgupta, S., 2013. Timescales of crustal melting in the Higher Himalayan Crystallines (Sikkim, Eastern Himalaya) inferred from trace element-constrained monazite and zircon chronology. *Contributions to Mineralogy and Petrology*, *165*(2), 349-372.

Schärer, U., 1984. The effect of initial 230Th disequilibrium on young UPb ages: the Makalu case, Himalaya. *Earth and Planetary Science Letters*, *67*(2), 191-204.

Shrestha, S., Larson, K. P., Guilmette, C., & Smit, M. A., 2017. The P–T–t evolution of the exhumed Himalayan metamorphic core in the Likhu Khola region, East Central Nepal. *Journal of Metamorphic Geology*, *35*(6), 663-693.

Scott, D. J., & St-Onge, M. R., 1995. Constraints on Pb closure temperature in titanite based on rocks from the Ungava orogen, Canada: Implications for U-Pb geochronology and PTt path determinations. *Geology*, *23*(12), 1123-1126.

Searle, M. P., & Godin, L. (2003). The South Tibetan detachment and the Manaslu leucogranite: A structural reinterpretation and restoration of the Annapurna-Manaslu Himalaya, Nepal. *The Journal of Geology*, *111*(5), 505-523.

Searle, M. P., Simpson, R. L., Law, R. D., Parrish, R. R., & Waters, D. J., 2003. The structural geometry, metamorphic and magmatic evolution of the Everest massif, High Himalaya of Nepal–South Tibet. *Journal of the Geological Society*, *160*(3), 345-366.

Simpson, R. L., Parrish, R. R., Searle, M. P., & Waters, D. J., 2000. Two episodes of monazite crystallization during metamorphism and crustal melting in the Everest region of the Nepalese Himalaya. *Geology*, *28*(5), 403-406.

Singer, J., Obermann, A., Kissling, E., Fang, H., Hetényi, G., and Grujic, D., 2017, Along-strike variations in the Himalayan orogenic wedge structure in Bhutan from ambient seismic noise tomography: Geochemistry, Geophysics, Geosystems, v. 18, p. 1483–1498, doi: 10.1002/2016GC006742.

Spencer, K.J., Hacker, B.R., Kylander-Clark, A.R.C., Andersen, T.B., Cottle, J.M., Stearns, M.A., Poletti, J.E., and Seward, G.G.E., 2013, Campaign-style titanite U-Pb dating by laser-ablation ICP: Implications for crustal flow, phase transformations and titanite closure: Chemical Geology, v. 341, p. 84–101, doi: 10.1016/j.chemgeo.2012.11.012.

Stacey, J.S., and Kramers, J.D., 1975, Approximation of terrestrial lead isotope evolution by a two-stage model: Earth and Planetary Science Letters, v. 26, p. 207–221, doi: 10.1016/0012-821X(75)90088-6.

Stearns, M.A., Hacker, B.R., Ratschbacher, L., Rutte, D., and Kylander-Clark, A.R.C., 2015, Titanite petrochronology of the Pamir gneiss domes: Implications for middle to deep crust exhumation and titanite closure to Pb and Zr diffusion: Tectonics, v. 34, p. 784–802, doi: 10.1002/2014TC003774.

Stearns, M.A., Cottle, J.M., Hacker, B.R., and Kylander-Clark, A.R.C., 2016, Extracting thermal histories from the near-rim zoning in titanite using coupled U-Pb and trace-element depth profiles by single-shot laser-ablation split stream (SS-LASS) ICP-MS: Chemical Geology, v. 422, p. 13–24, doi: 10.1016/j.chemgeo.2015.12.011.

Stephenson, N. and Cook. N., 1997. Metamorphic evolution of calcsilicate granulites near Battye Glacier, northern Prince Charles Mountains, East Antarctica. *Journal of Metamorphic Geology*, *15*(3), 361-378.

Thiede, R.C., and Ehlers, T.A., 2013, Large spatial and temporal variations in Himalayan denudation: Earth and Planetary Science Letters, v. 371–372, p. 278–293, doi: 10.1016/j.epsl.2013.03.004.

Treloar, P.J., and Coward, M.P., 1991, Indian Plate motion and shape: constraints on the geometry of the Himalayan orogen: Tectonophysics, v. 191, p. 189–198, doi: 10.1016/0040-1951(91)90055-W.

Van der Beek, P., Litty, C., Baudin, M., Mercier, J., Robert, X., and Hardwick, E., 2016, Contrasting tectonically driven exhumation and incision patterns, western versus central Nepal Himalaya: Geology, v. 44, p. 327–330, doi: 10.1130/G37579.1.

Vannay, J. C., & Grasemann, B., 1998. Inverted metamorphism in the High Himalaya of Himachal Pradesh (NW India): phase equilibria versus thermobarometry. *Schweizerische Mineralogische und Petrographische Mitteilungen*, *78*(1), 107-132.

Vannay, J. C., & Hodges, K. V., 1996. Tectonometamorphic evolution of the Himalayan metamorphic core between the Annapurna and Dhaulagiri, central Nepal. *Journal of Metamorphic Geology*, *14*(5), 635-656.

Vannay, J. C., Grasemann, B., Rahn, M., Frank, W., Carter, A., Baudraz, V., & Cosca, M., 2004. Miocene to Holocene exhumation of metamorphic crustal wedges in the NW Himalaya: Evidence for tectonic extrusion coupled to fluvial erosion. *Tectonics*, *23*(1).

Viskupic, K., Hodges, K. V., & Bowring, S. A., 2005. Timescales of melt generation and the thermal evolution of the Himalayan metamorphic core, Everest region, eastern Nepal. *Contributions to Mineralogy and Petrology*, *149*(1), 1-21.

Walker, J. D., Martin, M. W., Bowring, S. A., Searle, M. P., Waters, D. J., & Hodges, K. V., 1999. Metamorphism, melting, and extension: Age constraints from the High Himalayan slab of southeast Zanskar and northwest Lahaul. *The Journal of Geology*, *107*(4), 473-495.

Walters, J. B., & Kohn, M. J., 2017. Protracted thrusting followed by late rapid cooling of the Greater Himalayan Sequence, Annapurna Himalaya, central Nepal: Insights from titanite petrochronology. *Journal of Metamorphic Geology*, *35*(8), 897-917.

Warren, C. J., Grujic, D., Kellett, D. A., Cottle, J., Jamieson, R. A., & Ghalley, K. S., 2011. Probing the depths of the India-Asia collision: U-Th-Pb monazite chronology of granulites from NW Bhutan. *Tectonics*, *30*(2).

Warren, C. J., Hanke, F., & Kelley, S. P., 2012. When can muscovite 40Ar/39Ar dating constrain the timing of metamorphic exhumation?. *Chemical Geology*, *291*, 79-86.

Warren, C. J., Singh, A. K., Roberts, N. M., Regis, D., Halton, A. M., & Singh, R. B., 2014. Timing and conditions of peak metamorphism and cooling across the Zimithang Thrust, Arunachal Pradesh, India. *Lithos*, *200*, 94-110.

Webb, A. A. G., Yin, A., Harrison, T. M., Célérier, J., & Burgess, W. P., 2007. The leading edge of the Greater Himalayan Crystalline complex revealed in the NW Indian Himalaya: Implications for the evolution of the Himalayan orogen. *Geology*, *35*(10), 955-958.

Webb, A.A.G., Guo, H., Clift, P.D., Husson, L., Müller, T., Costantino, D., Yin, A., Xu, Z., Cao, H., and Wang, Q., 2017, The Himalaya in 3D: Slab dynamics controlled mountain building and monsoon intensification: Lithosphere, p. L636.1, doi: 10.1130/L636.1.

Yakymchuk, C., & Godin, L., 2012. Coupled role of deformation and metamorphism in the construction of inverted metamorphic sequences: an example from far-northwest Nepal. *Journal of Metamorphic Geology*, *30*(5), 513-535.

Yin, A., 2006, Cenozoic tectonic evolution of the Himalayan orogen as constrained by along-strike variation of structural geometry, exhumation history, and foreland sedimentation: Earth-Science Reviews, v. 76, p. 1–131, doi: 10.1016/j.earscirev.2005.05.004.

Zhang, L. S., & Schärer, U., 1996. Inherited Pb components in magmatic titanite and their consequence for the interpretation of U-Pb ages. *Earth and Planetary Science Letters*, *138*(1-4), 57-65.

FIGURE CAPTIONS

Figure 1: Geological map of the Himalaya (adapted from Kohn, 2014; Yin, 2006). Close up maps of sample location regions and U-Pb and Zr-in-titanite data from this study (a. Sutlej valley, b. western Nepal, c. Annapurna area, d. Langtang, e. Mt. Everest, f. eastern Nepal, g. Sikkim, h. western Bhutan and i. central Bhutan. Map based on a. Vannay and Grasemann, 1998; Webb et al., 2007; Chambers et al., 2008; Lederer et al., 2013; b. DeCelles et al., 1998; Carosi et al., 2007, 2010;Yakymchuk and Godin, 2012; Montimoli et al., 2013; He et al., 2015 c. Parsons et al., 2016a; d. Inger and Harris, 1993; Macfarlane, 1993; Kohn, 2008; e. Searle et al., 2003; Jessup et al., 2008; f. Groppo et al., 2009, 2013b; g. Mottram et al., 2014; h. Grujic et al., 2011; Warren et al., 2011, 2012; Kellett and Grujic, 2012; Regis et al., 2014; i. Grujic et al., 2011; Cooper et al., 2012.

Figure 2: Representative photomicrographs of samples analysed. (a) garnet-bearing calc-gneiss, (b) calc-silicate, (c) impure marble and d) amphibolite

Figure 3: Tera-Wasserburg plots summarizing the three main types of titanite U-Pb data yielded from this study, with representative chemical maps and trace element concentrations of titanite

grains: (a) single isochon population sample KL-8-11-8, (unanchored; 27 samples show this trend), (b) Sample SK12-216 with a spread of ages between two common-Pb anchored (Stacey and Kramers, 1975) intercepts (12 samples); (c) Sample 13-26, poorly-defined (unanchored) populations, with excess Pb analyses (8 samples). Tera-Wasserburg plots of each sample can be found in Supplementary Material S3.

Figure 4: Zr-in-titanite temperature data plotted against the ^{207}Pb corrected ^{206}Pb/^{238}U titanite date (Ma) for sample (a) DRB1233 (western Bhutan), (b) DRB1213 (western Bhutan) and (c) SK12-216 (Sikkim Himalaya).

Figure 5: (a) U-Pb titanite isochron dates and b) Zr-in-titanite temperatures of samples plotted with respect to their across strike position within the GHS relative to the MCT (0%) and the STD (100%).

Figure 6: Interpreted previously published P-T paths based on pseudosections (from metapelite samples proximal to samples analysed in this study), and previously published monazite data. The timing of core and rim U-Pb and Zr-in-titanite temperatures from titanite within this study are plotted for case study areas a) Kachenjunga, eastern Nepal (Ambrose et al., 2015) and Annapurna Nepal, (Iaccarino et al., 2015), b) Sikkim, India (Mottram et al., 2014) and d) Jomolhari, Bhutan (Regis et al., 2014).

Figure 7: Case study areas: (a) Annapurna, (b) Everest, (c) Eastern Nepal and (d) Jomolhari, showing titanite U-Pb Concordia dates (this study) compared to other published geochronological data (see references in Figure). Geology legends are the same as Fig. 1.

Figure 8. Compilation of along-strike age data from the central and eastern Himalaya. (a) Titanite data from this study is coloured by the average structural thickness of the Greater Himalayan Sequence (GHS) in each location. B) Summary of previously published monazite, titanite data and leucogranite data (from monazite and zircon data). References for previously published data are reported in Supplementary Table S3.

Figure 9: Summary of along-strike titanite U-Pb age trends for the oldest and youngest titanite from this study.

Figure 10: (a) Zr-in-titanite temperature, and (b) titanite U-Pb isochron age for each sample plotted against the average structural thickness of the GHS in that area and coloured by the along-strike longitudinal location of each sample.

Figure 11. Conceptual model showing schematic cross section across a) areas with a thick GHS where ductile accretion has occurred at depth, and (b) areas with a thinner GHS, where there has been less ductile accretion at depth and the development of a larger LHD. MFT= Main Frontal Thrust, MBT= Main Boundary Thrust, MCT= Main Central Thrust, GHS= Greater Himalayan Sequence and LHD= Lesser Himalayan Duplex. Adapted from Cottle et al., 2015a; Larson et al., 2015; Mercier et al., 2017.

TABLES

Table 1: Sample locations and mineral assemblages

Table 2: Summary of titanite U-Pb, Zr-in-titanite temperatures and trace element concentrations

Table 3: Lithology vs titanite age and temperature trends

Table 4: Comparison of differences in timing and temperatures of titanite crystallization in the different geological transects studied.

Table 5: Table 5: Comparison of differences in timing and temperatures of accessory phase crystallization ages in the different geological transects from a compilation of published HMC data.

SUPPLEMENTARY MATERIAL

Supplementary Table 1: Full U-Pb-Zr-REE dataset for all analysed titanite grains

Supplementary Table 2: Reference material reproducibility

Supplementary Table 3: Previously published petrochronology dataset

Supplementary Table 4: Zr-in-titanite temperatures

Supplementary Material S1: Detailed maps of titanite locations, temperatures, petrography and zoning

Supplementary Material S2: Detailed methods

Supplementary Material S3: Full Concordia diagrams, trace element profiles and Zr-in-titanite temperatures and data trends.

Table 1: Sample locations and mineral assemblages

Sample	Reference*	Area no. (Fig.1)**	Location				Rock type ***	Unit	Approx. map distance to (km)		dip ref	dip	STRUCT. THICK	PROPORTIO N	allanite	apatite	biotite	calcite	chlorite	clinopyroxene	epidote	Fe oxides	garnet	hornblende	K-feldspar	muscovite	orthopyroxene	plagioclase	quartz	Scapolite	titanite	zircon	Other
			Country	Location	Decimal Lat	Decimal Long			MCT	STD																							
402060	1	3	Nepal	Marysangdi valley	28.494	84.364	cg	UGHS	38	12	Vannay and Hodges, 1998	40	19	32	x	x		x		x	x	x		x	x			x	x	x	x	x	Hae, Py
402063	1	3	Nepal	Marysangdi valley	28.507	84.361	cg	UGHS	38	12	Vannay and Hodges, 1998	40	19	32	x	x		x		x	x	x		x	x			x	x	x	x	x	Py
05-55_	2	6	Nepal	Khumbu	27.850	86.783	cs	UGHS	25	20	Jessup et al., 2008	45	21	57				x		x					x		x	x	x	x	x	x	
06-57_	2	6	Nepal	Milke Danda	27.445	87.452	g-cs	LGHS	15	60	Groppo et al., 2009	35	29	85	x					x	x	x	x				x	x	x		x	x	
06-62_	2	6	Nepal	Milke Danda	27.398	87.450	g-cs	LGHS	10	60	Groppo et al., 2009	35	29	85			x			x		x	x					x	x		x	x	Gph
07-22_	2	6	Nepal	Makalu	27.798	87.126	cg	UGHS	25	20	schelling et al., 1992	40	27	62		x	x	x		x	x				x		x	x	x	x	x	x	
08-57_	2	6	Nepal	Mewa Khola	27.681	87.587	cg	UGHS	37	27	schelling et al., 1992	40	27	43				x	x	x	x	x			x			x	x		x	x	Sil
09-25_	2	6	Nepal	Khancenjunga	27.602	87.870	cg	UGHS	20	40	schelling et al., 1992	40	27	48				x		x		x		x				x			x	x	
10-37_	2	6	Nepal	lower Khumbu	27.620	86.719	g-cs	UGHS	5	40	Jessup et al., 2008	45	21	81			x				x	x	x	x				x	x		x	x	Sil
12-65_	2	6	Nepal	Dudh-Khunda	27.702	86.599	cg	UGHS	20	40	Jessup et al., 2008	45	25	80	x	x		x		x	x	x		x	x			x	x	x	x	x	Hae, Gph
13-26_	2	6	Nepal	Singalilla Ridge	27.106	87.992	g-cs	LGHS	10	65	schelling et al., 1992	40	27	85	x					x		x	x					x	x		x	x	Gph
14-17b_	2	4	Nepal	Langtang	28.197	85.617	cg	UGHS	20	15	Fraser et al., 2000	45	30	51						x	x				x			x	x		x	x	
14-44c_	2	4	Nepal	Gosaikund	28.087	85.393	cs	UGHS	2	33	Fraser et al., 2000	45	30	84				x		x		x	x	x		x		x	x		x	x	
14-74b_	2	4	Nepal	Gosaikund	27.849	85.459	g-cs	UGHS	3	32	Fraser et al., 2000	45	30	73			x				x		x	x	x			x	x		x	x	Tur
B126	3	9	Bhutan	C/E Bhutan- Jakar	27.511	90.286	m	UGHS/TSS	69.9	0.1	Kellett et al., 2010 ish	30	30	2		x	x	x		x	x					x		x			x	x	
BU14-137	16	9	Bhutan	N. Central Bhutan	27.826	90.491	cg	UGHS	65	5	Kellett et al., 2010 ish	30	30	7				x		x	x			x				x	x		x	x	
CWB-10-2	4	8	Bhutan	Gasa	27.910	89.734	cg	LGHS	60	15	Average	40	27	28	x	x			x	x	x		x	x				x	x		x	x	
D13-49B	5	2	Nepal	Mugu Karnali	29.661	82.625	a	UGHS/TSS	?	1	Montimoli et al., 2013	45	18	4		x	x			x	x			x	x			x	x		x	x	
DH12-4-10-4	6	2	Nepal	Dadeldhura klippe	29.253	82.132	m	UGHS	15	6	Robinson et al., 2006	40	15	34			x	x				x				x			x		x	x	Rt
DH12-5-10-11	6	2	Nepal	Dadeldhura klippe	29.236	82.061	cg	UGHS	23	4	Robinson et al., 2006	40	15	23	x	x	x	x		x	x	x		x				x	x	x	x	x	Hae
DH12-6-10-3	6	2	Nepal	Dadeldhura klippe	29.228	82.013	m	UGHS	35	1	Robinson et al., 2006	40	15	5	x	x	x	x		x	x	x						x	x		x	x	
DRB1213	7	8	Bhutan	Far western Bhutan	27.741	89.266	m	UGHS	24.9	0.1	Kellett and Grujic, 2012	40	19	2	x	x	x	x		x	x	x			x			x	x	x	x	x	Hae
DRB1219	7	8	Bhutan	Far western Bhutan	27.736	89.291	g-cs	UGHS	24.9	0.1	Kellett and Grujic, 2012	40	19	2						x			x					x	x		x	x	
DRB1233	7	8	Bhutan	Far western Bhutan	27.797	89.350	cs	UGHS	24.8	0.2	Kellett and Grujic, 2012	40	19	2	x	x	x	x		x	x					x			x	x	x	x	Fl
ET-16	8	5	Nepal	Hermit's gorge	28.141	86.876	a	UGHS	64.8	0.2	Jessup et al., 2008	30	30	6							x		x	x				x	x		x	x	
FB118	9	8	Bhutan	Far western Bhutan	27.780	89.339	m	UGHS	24.8	0.2	Kellett and Grujic, 2012	40	19	2	x	x		x		x						x			x		x	x	
FB123	9	9	Bhutan	C/E Bhutan- Jakar	27.512	90.284	m	UGHS/TSS	59.1	0.1	Kellett et al., 2010 ish	30	30	0.5			x	x			x					x			x		x	x	
FB72	9	9	Bhutan	C Bhutan, Punakha	27.609	89.938	cg	UGHS	58	2	Kellett et al., 2010 ish	30	30	4	x	x		x		x	x			x				x	x		x	x	Ccp
K09-25c	11	1	India	Manikaran	32.005	77.410	g-cs	LGHS	2	3	webb et al., 2007	30	4	88			x				x		x			x			x		x	x	
K09-65a	11	1	India	Sutlej- Ribba	31.581	78.387	a	UGHS	24	3	Caddick et al., 2007	30	17	10	x	x	x		x			x	x	x				x	x		x	x	
K09-75d	11	1	India	Sutlej- Poo	31.767	78.637	cs	GHS?	?	3	Caddick et al., 2007	30	17	10	x					x	x	x	x	x		x	x	x	x	x	x	x	
KL-4-11-5	5	3	Nepal	Kali Gandaki	28.628	83.582	a	UGHS	22	3	Parsons et al., 2014	30	17	10	x	x	x						x	x				x	x		x	x	
KL-8-11-8	5	3	Nepal	Kali Gandaki	28.629	83.594	a	UGHS	22	3	Parsons et al., 2014	30	17	10			x	x						x					x		x	x	tur
MK14	12	3	Nepal	Modi Kohlar	28.471	83.869	cs	UGHS	23	2	Parsons et al., 2014	40	19	28			x	x		x	x	x							x		x	x	
MK15	12	3	Nepal	Modi Kohlar	28.507	83.904	cg	UGHS	23	2	Parsons et al., 2014	40	19	28	x		x			x	x			x	x	x		x	x	x	x	x	
MK9	12	3	Nepal	Modi Kohlar	28.471	83.869	a	UGHS	15	10	Parsons et al., 2014	40	19	28	x	x	x	x						x				x	x	x	x	x	
P12/048	13	3	Nepal	Kali Gandaki	28.590	83.648	m	UGHS	15	10	Parsons et al., 2014	30	17	34			x	x				x				x			x	x	x	x	Rt, Tur
P12/054	13	3	Nepal	Kali Gandaki	28.616	83.638	cg	UGHS	20	5	Parsons et al., 2014	30	17	17	x	x	x	x			x			x				x	x		x	x	Tur
P13/031	13	3	Nepal	Kali Gandaki	28.665	83.583	a	UGHS	24	1	Parsons et al., 2014	30	17	3				x		x	x	x		x				x	x		x	x	
R03-36	8	5	Nepal	Hermit's gorge	28.161	86.880	s	UGHS	64.8	0.2	Jessup et al., 2008	30	30	1			x					x		x				x	x		x	x	
R03-40	8	5	Nepal	Hermit's gorge	28.166	86.880	s	UGHS	64.8	0.2	Jessup et al., 2008	30	30	0.5			x					x		x		x		x	x		x	x	
R03-69	8	5	Nepal	Hermit's gorge	28.141	86.876	s	UGHS	64.8	0.2	Jessup et al., 2008	30	30	1			x					x		x				x	x		x	x	
R03-71	8	5	Nepal	Hermit's gorge	28.141	86.876	s	UGHS	64.8	0.2	Jessup et al., 2008	30	30	3			x					x		x				x	x		x	x	
SK12-119	14	7	Sikkim	Lava- Neora	27.084	88.674	cg	LGHS	7	60	Mottram, 2014	30	30	95	x	x	x	x						x					x	x	x	x	Ccp, Sil
SK12-216	14	7	Sikkim	Pelling-Yuksom	27.363	88.204	cg	LGHS	3	50	Mottram, 2014	35	30	95	x	x	x	x					x	x	x				x	x	x	x	
SK12-344	14	7	Sikkim	Mirik-Darjeeling	27.007	88.212	cg	LGHS	10	60	Mottram, 2014	35	30	85	x			x	x			x						x	x	x	x	x	Ccp

Table 2: Summary of titanite U-Pb, Zr-in-titanite temperatures and trace element concentrations

Sample	Transect[1]	Rock type[2]	Comment	Ttn diameter (µm)	Number of laser analyses	(Ma) Date[3]	± 2σ[4]	MSWD	Excess Pb?[5]	T (°C)[6]	2σ[7]	2σi[8]	Average trace element concentrations (ppm) Th/U	U	Th	Pb	Y	2SE	Zr	2SE	Fe	2SE	Nb	2SE	Normalised[9] Nd	Eu*	Yb/Gd
402060	C	cg	cores/ larger grains	250-500	16	22.4	0.7	1.9		752	41	16	0.4	110.2	39.8	0.9	1058	96	230	24	3691	337	579	55	1201.7	0.6	0.6
402060	C	cg	rim/ small grains	250-500	7 (+7 others)	19	0.9	6.4	3.4	751	40	14	0.5	118.3	65.4	1.0	1145	89	237	23	4149	454	516	51	1564.6	0.6	0.7
402063	C	cg	cores/ larger grains	250-1000	20	27.4	1.6	4.8		737	39	14	0.2	98.2	22.3	1.1	794	74	180	16	3606	343	712	70	670.5	0.9	0.7
402063	C	cg	mainly rim, Eu anom	250-1000	6 (+10 others)	18.2	1.9	4	9.2	743	40	15	0.3	125.6	50.3	1.0	830	84	208	18	4890	447	773	69	30.3	0.9	0.9
05-55_	F	cs	single population	100-300	47	21.8	1.3	0.7		711	42	17	1.6	62.5	102.0	3.4	310	34	253	28	4155	609	919	106	609.1	0.8	0.4
06-57_	F	g-cs	some inherited grains	50-200	42	12.5	8.4	1	Yes	743	39	17	0.0	6.8	0.4	2.4	220	24	140	20	1373	363	1522	171	52.0	1.0	1.1
06-62_	F	g-cs	some inherited grains	100-200	26	15.3	0.7	1.2	Yes	753	41	15	0.1	37.5	3.9	1.4	262	18	357	26	1215	363	1565	100	171.2	1.1	0.5
07-22_	F	cg	cores	100-800	12	18.8	1.4	7		808	45	16	3.4	187.6	629.4	1.8	379	30	813	51	2294	246	1053	69	874.0	0.6	0.4
07-22_	F	cg	rims	100-800	6 (+27 others)	12	0.5	0.7	6.8	770	43	13	1.3	156.4	229.6	0.8	738	57	555	47	1808	184	1052	83	1488.4	0.6	0.4
08-57_	F	cg	single population	400-800	48	17.4	1.7	0.4		814	45	16	6.3	74.1	480.3	3.4	1310	96	761	65	3454	352	1073	87	3339.8	0.4	0.6
09-25_	F	cg	single population	100-300	48	13.7	0.5	0.9		806	44	15	1.9	174.7	288.0	1.4	1497	110	654	52	2374	264	1584	126	2675.3	0.5	0.7
10-37_	F	g-cs	some inherited grains	100-200	37	19	6.5	1.9	Yes	686	40	18	0.2	8.6	1.1	1.8	662	58	115	13	1727	424	4021	365	57.0	0.8	2.5
12-65_	F	cg	no clear relationship	100-400	7	25.5	4.1	6.6		740	40	15	3.0	68.3	24.4	1.0	1270	109	194	23	2239	397	1195	138	1227.3	0.5	0.8
12-65_	F	cg	no clear relationship	100-400	7 (+32 others)	15	3.1	8.5	10.5	723	45	18	0.4	126.0	377.2	1.0	1405	133	822	77	3720	549	839	97	3369.8	0.6	0.6
13-26_	F	g-cs	some inherited grains	100-200	41	12.4	5	0.8	Yes	754	39	16	0.1	13.8	0.9	1.7	167	22	134	16	1988	655	2597	293	58.4	0.7	0.6
14-17b_	D	cg	single population	300-800	46	19.2	0.5	2		785	44	16	2.4	99.9	236.9	4.3	1106	90	555	49	3807	371	684	57	2283.3	0.6	0.8
14-44c_	D	cs	some inherited grains	100-200	30	14	3.3	0.3	Yes	716	38	16	0.1	12.1	0.2	4.7	128	12	113	11	623	428	7823	830	57.3	1.0	0.2
14-74b_	D	g-cs	single population	200-300	40	17.9	1.4	0.7		748	40	16	0.1	8.0	0.3	1.6	142	15	234	24	1665	396	1837	198	36.4	1.5	0.4
B126	I	m	single population	100-300	44	15.5	0.8	2.4		658	38	16	0.1	18.2	2.1	1.6	164	16	102	12	1269	424	1009	134	117.2	0.7	0.7
BU14-137	I	cg	single population	200-450	21	16	2.1	1		730	40	17	0.1	5.9	0.6	0.3	513	60	187	23	7343	985	1220	142	36.6	0.7	10.9
CWB-10-2	H	cg	rim/core/small	200-450	10	14.4	1.4	7		770	41	16	1.0	183.2	199.5	1.8	1638	150	368	31	2753	223	803	67	2944.4	0.5	0.5
CWB-10-2	H	cg	rims	200-450	13 (+13 others)	12.6	0.4	3.7	1.8	764	40	14	1.4	110.8	176.3	1.4	1429	117	319	28	3158	265	501	44	2273.5	0.5	0.7
D13-49B	B	a	single population	100-300	34	18.8	1.5	1.3		710	38	16	0.4	10.1	5.3	0.8	576	57	146	17	3334	648	5852	576	93.8	0.7	2.1
DH12-4-10-4	B	m	single population	100	26	16.6	2.7	0.3		738	38	15	0.2	23.8	2.6	1.9	395	32	183	19	1513	331	3197	275	357.3	0.8	0.5
DH12-5-10-11	B	m	core and rim	300-750	7	26.5	1.8	10.5		740	39	13	0.9	154.3	137.7	0.8	432	33	172	13	2774	187	629	49	889.7	0.7	0.4
DH12-5-10-11	B	cg	rims	300-750	5 (+6 others)	18.3	2	4.7	8.2	735	38	13	0.5	152.4	67.3	1.0	492	40	156	10	2708	208	571	42	908.1	0.6	0.4
DH12-6-10-3	B	m	single population	100	40	20	0.7	1.3		735	41	15	0.1	119.3	14.6	3.4	1079	90	165	15	2687	482	3155	264	788.5	0.7	0.7
DRB1213	H	m	cores and rims	100	9	21.9	0.6	2		733	41	15	0.8	127.5	105.3	1.3	681	50	171	16	1014	106	714	56	1033.9	0.4	0.7
DRB1213	H	m	small grains	100	8 (+ 14 others)	13.1	0.5	0.6	8.8	716	38	13	1.4	103.9	280.4	2.8	679	44	127	9	1118	89	565	45	1364.0	0.4	0.6
DRB1219	H	g-cs	single population	100-400	33	18.2	2.3	0.8		730	38	14	0.0	5.2	0.2	1.2	112	11	179	13	1604	124	687	55	20.8	0.8	1.0
DRB1233	H	cs	rims and cores	200-750	18	19.6	1.3	2.8		757	39	12	0.4	69.0	30.1	1.6	1126	76	198	14	2096	173	1044	88	710.2	0.5	0.9
DRB1233	H	cs	small grains	200-750	7 (+7 others)	16.1	0.9	3.2	3.5	779	41	14	0.7	101.1	85.4	1.3	1232	93	304	24	2186	183	534	41	1392.3	0.5	0.6
ET-16	E	a	single population	100-200	34	15.2	0.9	3.6		672	38	13	0.5	55.4	28.5	1.1	836	62	100	7	9335	799	560	44	461.1	0.7	0.9
FB118	H	m	cores/ larger grains	200-300	16	19	0.6	2.6		791	41	16	1.5	141.5	223.9	5.4	462	40	420	43	670	398	1212	123	1230.0	0.5	0.5
FB118	H	m	rims	200-300	27	14.3	1.3	2.2	4.7	742	38	14	1.3	106.0	134.2	13.6	691	66	150	16	801	446	643	66	1216.0	0.4	0.6

FB123	I	m	single population	100-200	46	17.2	0.7	4.3		626	38	18	0.2	51.5	8.6	3.4	152	12	37	6	1129	411	669	56	348.4	0.6	0.3
FB72	I	cg	single population	300-700	43	14.9	0.8	1.6		715	42	15	0.3	37.9	13.3	0.7	842	67	248	21	2329	436	1034	93	569.4	0.7	0.8
K09-25c	A	g-cs	some inherited grains	100-200	21	21.4	3.9	1.3	Yes	657	36	17	0.5	26.0	9.2	12.4	935	102	29	5	4559	613	565	63	171.9	1.0	2.2
K09-65a	A	a	single population	100	38	22.8	1.7	2.8		695	36	14	0.1	20.5	3.4	2.2	837	73	80	8	3294	598	651	58	190.7	0.7	1.2
K09-75d	A	cs	single population	100-200	44	20.5	2.9	0.3		700	37	15	0.2	19.7	3.5	2.3	556	54	94	10	1421	374	1222	122	239.7	1.1	0.5
KL-4-11-5	C	a	some inherited grains	200-300	35	31	10	74	Yes	734	37	15	0.7	34.1	23.0	1.4	914	83	129	16	4126	555	1620	152	363.0	1.0	2.6
KL-8-11-8	C	a	single population	1000	45	24	0.8	0.9		766	39	16	0.1	100.7	87.9	4.6	484	51	201	22	6810	941	4284	452	803.7	0.4	0.6
MK14	C	cs	single population	100-300	48	22.6	0.9	2.8		780	40	15	0.8	77.9	33.4	1.5	68	295	25	2053	1836	376	2053	210	1055.6	0.7	0.4
MK15	C	cg	cores and rims	200-500	10	24.5	1.5	1.3		778	41	15	0.1	26.3	2.8	0.8	661	45	317	22	1784	154	688	47	228.3	0.7	1.0
MK15	C	a	cores and rims	200-500	16 (+4 others)	18.2	1.2	4.1		739	38	13	0.1	32.7	2.9	1.2	630	41	140	10	2043	195	628	51	239.0	0.8	1.0
MK9	C	m	some inherited grains	100-200	47	18.9	1.3	1	Yes	759	39	15	0.2	88.0	19.8	3.5	91	191	20	2222	3628	538	2222	264	569.8	0.7	1.3
P12/048	C	m	single population	300-700	46	23.4	5.6	0.2		678	36	14	0.2	40.6	6.9	13.8	583	46	77	7	1526	420	1517	148	410.5	0.8	0.5
P12/054	C	cg	single population	100-300	32	20	1	4.5		743	40	15	0.2	78.4	12.9	1.1	1423	126	205	17	3312	496	1501	136	765.7	0.8	1.1
P13/031	C	a	single population	100-300	42	28	11	0.2		747	37	13	0.2	2.3	0.7	2.5	373	25	168	12	6020	499	1084	85	40.9	0.8	6.1
R03-36	E	as	single population	100-300	30	19.1	1.6	1.1		687	41	19	0.2	19.6	5.9	1.7	722	109	144	21	6250	1192	540	88	235.6	0.8	2.1
R03-40	E	as	single population	100	35	18.8	2.5	0.3		665	40	19	0.2	29.4	8.4	7.2	1539	236	111	17	15364	2875	758	122	165.5	1.0	3.1
R03-69	E	as	single population	100-200	28	15.6	0.5	1.5		677	41	19	0.1	99.0	11.4	3.3	4338	691	113	17	11620	3113	1277	207	629.4	0.7	2.9
R03-71	E	as	single population	100-300	44	16.9	0.6	1.2		680	41	20	0.1	46.1	7.1	1.6	952	165	121	19	14479	2060	739	122	331.7	0.7	2.4
SK12-119	G	cg	single population	100-300	40	14.8	0.5	1		742	39	14	0.7	256.0	122.2	13.2	2489	196	195	14	3575	358	1185	94	1196.4	1.0	1.7
SK12-216	G	cg	mainly cores	200-500	12	22.3	0.7	2.6		748	38	13	1.6	148.7	252.9	0.7	216	16	224	17	5676	424	382	28	1148.1	0.6	0.1
SK12-216	G	cg	rims	200-500	8 (+8 others)	15.4	1.2	3.4	6.9	757	40	14	1.7	157.1	259.2	0.6	629	42	308	24	5596	464	24	609	1237.3	0.6	0.5
SK12-344	G	cg	single population	200-500	40	18.7	1.2	0.6		762	38	13	0.2	59.5	14.1	1.8	635	39	190	12	3986	233	546	35	405.5	0.8	0.8
TH-B12-IG05	H	cg	cores	200-500	10	19.1	2	6.2		773	41	15	0.5	305.3	362.9	2.1	1277	68	356	21	2442	148	526	26	3838.4	0.4	0.4
TH-B12-IG05	H	cg	rims	200-500	15(+15 others)	15.3	1.3	6.6	3.8	744	38	13	1.2	192.0	95.5	1.9	1255	99	210	12	2584	153	654	38	1670.0	0.6	0.6

1. A= Sutlej valley area NW India, B= Western Nepal, C=Annapurna, Nepal, D= Langtang, E= Everest, F= Kachenjunga and Eastern Nepal, G= Sikkim, H= Jomolhari, Western Bhutan, I= Central Bhutan

2. Rock type- a= amphibolite, as= amphibolite schist, cg= calc-gniess, cs= calc-silicate, g-cs= garnet-bearing calc silicate, m= impure marble.

3. U-Pb isochron date (unanchored except for samples which yield a spread of ages [highlighted in light grey in table] which were anchored at 0.83±0.02- Stacey and Kramers, 1975 common-Pb composition)

4. Uncertainties includes in-run errors, decay constant errors and propogated uncertainties for reproducibility of secondary reference materials FC and Y1710C5

5. Approximate date of inherited titanite analyses

6. Zr-in-titanite temperature (Hayden et al., 2008)

7. Uncertainties includes propogated analytical uncertainties, and additional uncertainties for errors in pressure determination and activity of rutile (for comparing with external results.

8. Uncertaintie include propogated analytical uncertainties and additional uncertainty for errors in pressure determination (for comparing samples internally)

9. Normalised to McDonough and Sun, 1995

Table 3: Lithology vs titanite age and temperature trends

Rock type	n	Single	Spread	Excess Pb	Average titanite date (Ma)	2σ	Oldest titanite date (Ma)	2σ	Youngest titanite date (Ma)	2σ	Average Zr-in-ttn T (°C)	2σi	Maximum Zr-in-ttn T (°C)	2σi	Minimum Zr-in-ttn T (°C)	2σi
Amphibolite	10	9	0	1	21	3.1	31	10	15.2	0.9	703	16	766	16	665	19
Marble	9	5	3	1	18.7	1.5	26.5	1.8	13.1	0.5	721	15	791	16	626	18
Calc-gneiss	16	8	8	0	18.1	1.4	27.4	1.6	12	0.5	758	15	814	16	715	15
Calc-silicate	12	5	1	6	17.8	3	22.6	0.9	12.4	5	732	16	780	15	657	17

Table 4: Comparison of differences in timing and temperatures of titanite crystallization in the different geological transects studied.

Location	δt[1] (Ma)	δT[2] (°C)	Average thickness of GHS (km)	Average structural location (no unit)[3]	Average Longitude (decimal degree)	Oldest titanite date (Ma)	2σ ab	Youngest titanite date (Ma)	2σ ab	Highest Zr-in-titanite T (°C)	2σ ab	Lowest Zr-in-titanite T (°C)	2σ ab
Sutlej valley	2.3	43	13	36.0	78.1443	22.8	1.7	20.5	2.9	700	15	657	17
Western Nepal	12.0	30	16	17.6	82.1785	28.6	1.7	16.6	2.7	740	13	710	16
Kali Gandaki	13.1	102	15	17.0	84.3627	31.0	10.0	17.1	1.1	752	16	737	14
Modi Khola	9.9	15	19	23.7	83.7325	22.9	0.6	17.9	1.0	780	15	678	14
Langtang	5.4	69	30	69.4	85.4898	19.2	0.5	13.8	3.3	785	16	716	16
Everest	4.4	22	30	2.3	86.8777	19.1	1.6	15.6	0.5	687	19	665	19
Eastern Nepal	16.0	128	26	69.7	87.2092	28.2	7.2	12.5	0.7	814	16	686	18
Sikkim	7.6	20	29	92.8	88.3237	21.9	1.1	14.3	1.0	757	14	742	14
Jomolhari	8.8	64	19	2.0	89.7302	26.6	2.9	12.5	0.4	773	15	744	13
Laya	14.1	26	27	28.1	89.3143	23.0	0.5	13.2	0.5	791	16	716	13
Central Bhutan	2.3	72	30	3.2	90.2495	17.2	0.7	14.9	0.8	730	17	626	18

1. δt = duration of metamorphism, the difference between maximum and minimum titanite U-Pb age in each section
2. δT= difference between maximum and minimum titanite Zr-in-titanite temperature in each section
3. Average structural location= structural location within the GHS in relation to the STD (0) and the MCT (100).

Table 5: Comparison of differences in timing and temperatures of accessory phase crystallization ages in the different geological transects from a compilation of published HMC data.

Location[1]	Average Longitude (decimal degree)	Oldest Mnz/ttn date (Ma)	2σ ab	Youngest mnz/ttn date (Ma)	2σ ab	Duration	2σ ab	n=
Sutlej valley	78.606	29	0.2	17.9	0.1	11.1	0.2	28
Karnali Klippe, Western Nepal	81.931	53.3	3.9	9.2	0.2	44.1	3.9	26
Upper/Mugu Karnali, Western Nepal	82.435	41.4	3.9	17	0.2	24.4	3.9	15
Kali Gandaki	83.614	48.8	2	20	0.9	28.8	2.2	9
Modi Khola	83.856	40.3	2	17.9	0.9	22.4	2.2	21
Marysangdi Valley	84.327	33.2	1.4	14.5	0.3	18.7	1.4	29
Langtang	85.452	32.4	0.7	12.8	1.1	19.6	1.3	22
Tami Khosi	86.369	26	0.5	14.6	0.5	11.4	0.7	20
Everest	86.822	32.2	0.4	15	0.1	17.2	0.4	27
Makalu-E	87.227	38.9	0.9	12	0.4	26.9	1.0	26
Kachenjunga	87.824	41.5	0.9	12.4	0.4	29.1	1.0	19
Sikkim	88.555	36.4	0.9	13.1	0.4	23.3	1.0	52
Jomolhari	89.277	36.1	0.9	13.1	0.4	23	1.0	17
Laya	89.65	24.2	0.9	13.3	0.4	13.9	1.0	24
Central Bhutan	90.517	24.5	0.7	12.5	0.4	12	0.8	19
Eastern Bhutan	91.062	26	0.9	14.5	0.4	11.5	1.0	8
Arunarchal	91.745	27.3	0.9	11.5	0.4	15.8	1.0	12

1. Data from: This study; Ambrose et al., 2015; Bardden et al., 2017; Carosi et al., 2010; 2016; Catlos et al., 2001; 2004; Corrie and Kohn, 2011; Cottle et al., 2009; 2015; Daniel et al., 2003; Edwards and Harrison, 1997; From et al., 2014; Groppo et al., 2010; Harrison et al., 1995; 1997; Hodges et al., 1998; Jessup et al., 2008; Kellett et al., 2010; 2013; Kohn and Corrie, 2011; Kohn et al., 2004; Larson and Cottle, 2014; Larson et al., 2013; Lederer et al., 2013; Leloup et al., 2010; Montimoli et al., 2013; Mottram et al., 2014; 2015; Murphy and Harrison, 1999; Regis et al., 2014; 2016; Rubatto et al., 2013; Scharer et al., 1986; Searle et al., 2003; Simson et al., 2000; Soucy La Roche et al., 2017; Streule et al., 2010; Tobgay et al., 2012; Walters and Kohn, 2017; Warren et al., 2011; 2012; 2014; Zeiger et al., 2015.

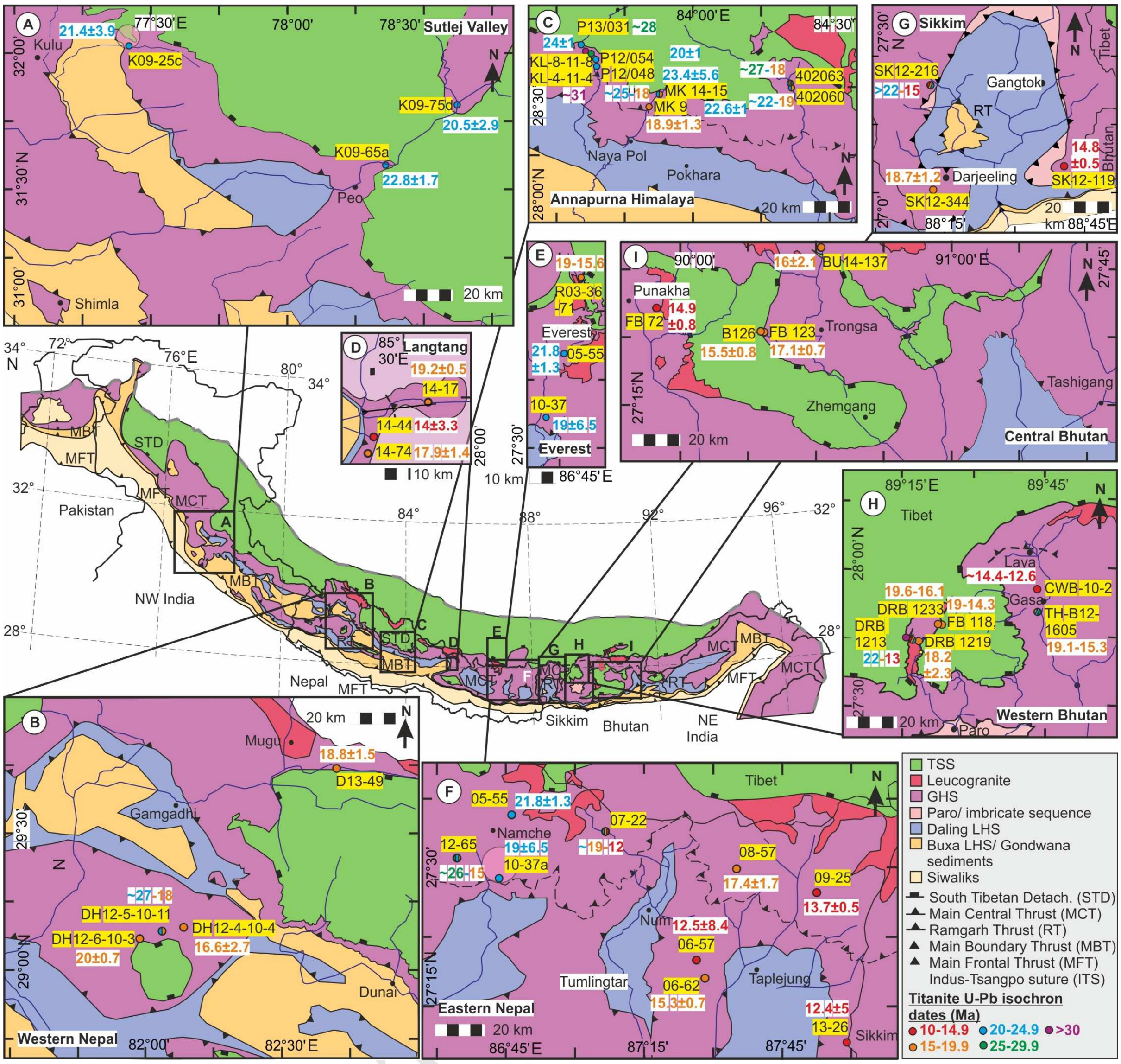

A
Sutlej Valley
77°30'E
78°00'
78°30'
21.4±3.9
Kulu
K09-25c
K09-75d
20.5±2.9
K09-65a
22.8±1.7
Peo
Shimla
32°00'
31°30'N
31°00'
20 km
C
84°00'E
84°30'
P13/031 ~28
24±1
KL-8-11-8
KL-4-11-4
P12/054
P12/048
~31
20±1
23.4±5.6
~27-18
402063
402060
~25-18
MK 14-15
MK 9
18.9±1.3
22.6±1
~22-19
28°30'
Naya Pol
Pokhara
Annapurna Himalaya
28°00'N
20 km
G
Sikkim
SK12-216
>22-15
Gangtok
RT
14.8
±0.5
SK12-119
18.7±1.2
Darjeeling
SK12-344
27°30'N
27°0'
88°15'
20 km
88°45'E
Tibet
Bhutan
E
19-15.6
R03-36
-71
Everest
21.8
±1.3
05-55
10-37
19±6.5
Everest
27°30'
10 km
86°45'E
I
90°00'
91°00'E
16±2.1
BU14-137
Punakha
FB 72
14.9
±0.8
B126
FB 123
Trongsa
15.5±0.8
17.1±0.7
27°15'N
27°45'
Zhemgang
Tashigang
20 km
Central Bhutan
D
Langtang
85°30'E
19.2±0.5
14-17
14-44
14±3.3
14-74
17.9±1.4
28°00'
10 km
34°
72°
76°E
80°
34°
N
MBT
MFT
STD
32°
Pakistan
MFT
MCT
A
84°
88°
92°
96°
32°
NW India
MBT
B
C
28°
STD
MBT
RT
D
E
G
H
I
28°
Nepal
MFT
MCT
F
MCT
RT
Sikkim
Bhutan
MBT
MCT
MFT
MCT
NE India
H
89°15'E
89°45'
Tibet
28°00'N
Lava
~14.4-12.6
CWB-10-2
Gasa
19.6-16.1
DRB 1233
19-14.3
FB 118
TH-B12-1605
DRB 1213
22-13
DRB 1219
18.2
±2.3
19.1-15.3
27°30'
20 km
Paro
Western Bhutan
B
20 km
Mugu
18.8±1.5
D13-49
Gamgadhi
29°30'
~27-18
DH12-5-10-11
DH12-6-10-3
DH12-4-10-4
20±0.7
16.6±2.7
Dunai
29°00'N
Western Nepal
82°00'
82°30'E
F
Tibet
05-55
21.8±1.3
07-22
Namche
12-65
19±6.5
~19-12
08-57
10-37a
~26-15
17.4±1.7
09-25
13.7±0.5
27°30'
Num
12.5±8.4
06-57
Tumlingtar
06-62
15.3±0.7
Taplejung
12.4±5
13-26
Sikkim
27°15'N
Eastern Nepal
20 km
86°45'E
87°15'
87°45'
TSS
Leucogranite
GHS
Paro/ imbricate sequence
Daling LHS
Buxa LHS/ Gondwana sediments
Siwaliks
South Tibetan Detach. (STD)
Main Central Thrust (MCT)
Ramgarh Thrust (RT)
Main Boundary Thrust (MBT)
Main Frontal Thrust (MFT)
Indus-Tsangpo suture (ITS)
Titanite U-Pb isochron dates (Ma)
10-14.9
20-24.9
>30
15-19.9
25-29.9

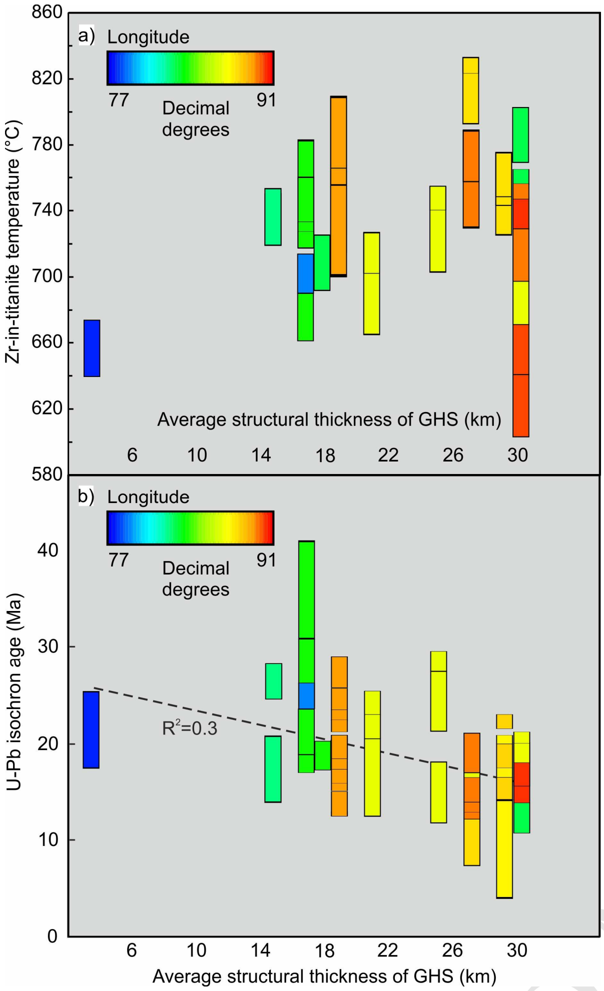
a) Longitude
77
91
Decimal degrees
Zr-in-titanite temperature (°C)
860
820
780
740
700
660
620
580
Average structural thickness of GHS (km)
6
10
14
18
22
26
30
b) Longitude
77
91
Decimal degrees
U-Pb isochron age (Ma)
40
30
20
10
0
R²=0.3
6
10
14
18
22
26
30
Average structural thickness of GHS (km)

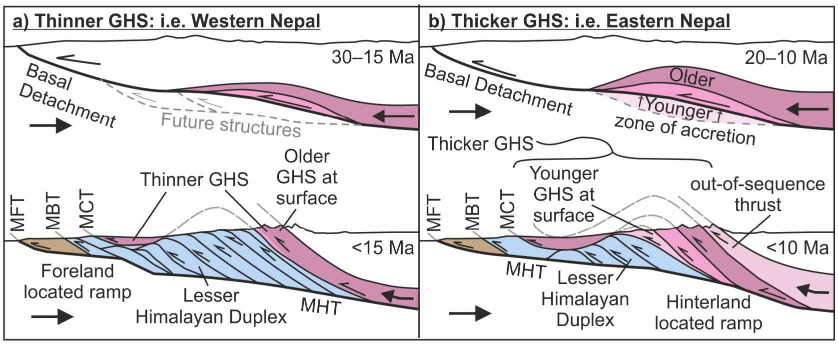
a) Thinner GHS: i.e. Western Nepal
30–15 Ma
Basal Detachment
Future structures
Thinner GHS
Older GHS at surface
MFT
MBT
MCT
<15 Ma
Foreland located ramp
Lesser Himalayan Duplex
MHT
b) Thicker GHS: i.e. Eastern Nepal
20–10 Ma
Basal Detachment
Older
Younger
zone of accretion
Thicker GHS
Younger GHS at surface
out-of-sequence thrust
MFT
MBT
MCT
<10 Ma
MHT
Lesser Himalayan Duplex
Hinterland located ramp

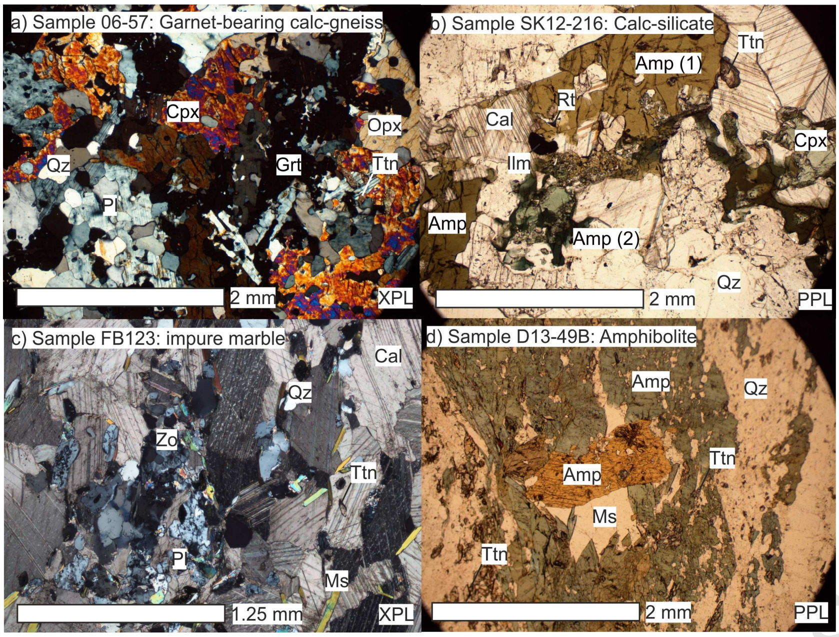
a) Sample 06-57: Garnet-bearing calc-gneiss
Cpx
Opx
Qz
Grt
Ttn
Pl
2 mm
XPL
b) Sample SK12-216: Calc-silicate
Ttn
Amp (1)
Rt
Cal
Cpx
Ilm
Amp
Amp (2)
Qz
2 mm
PPL
c) Sample FB123: impure marble
Cal
Qz
Zo
Ttn
Pl
Ms
1.25 mm
XPL
d) Sample D13-49B: Amphibolite
Amp
Qz
Ttn
Amp
Ms
Ttn
2 mm
PPL

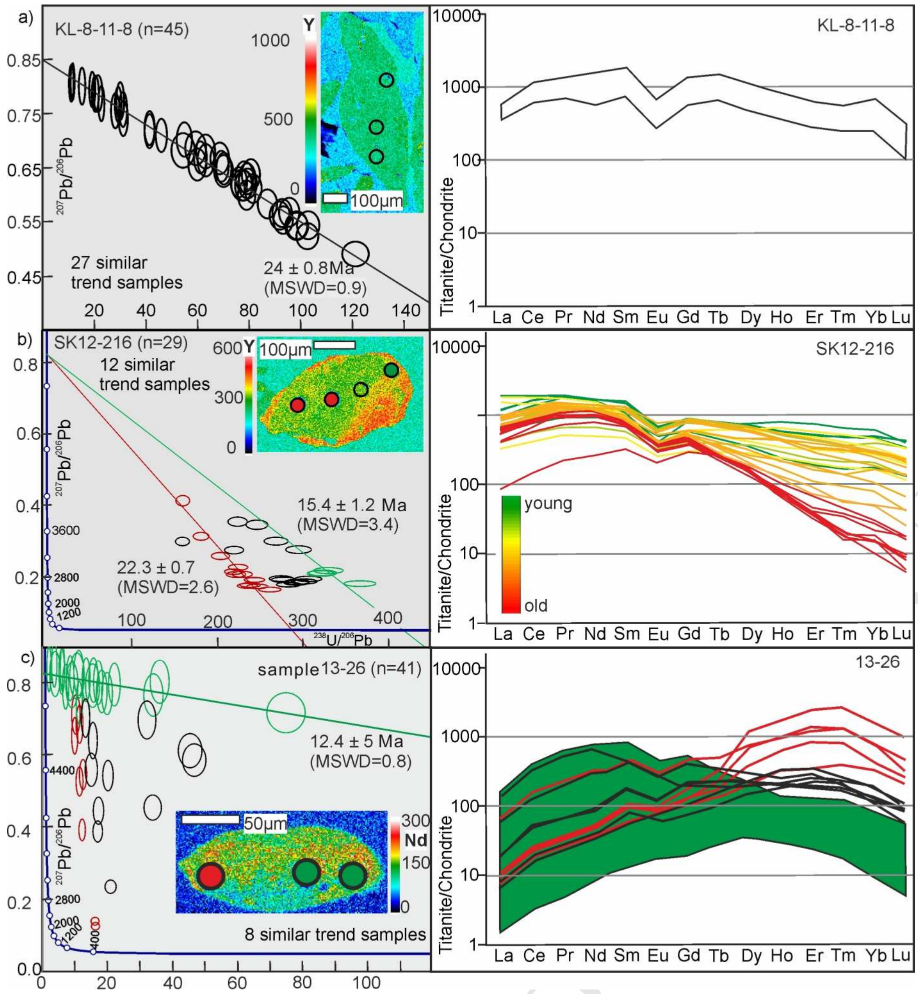

a)
KL-8-11-8 (n=45)
27 similar trend samples
24 ± 0.8Ma (MSWD=0.9)
100µm
KL-8-11-8
Titanite/Chondrite
La Ce Pr Nd Sm Eu Gd Tb Dy Ho Er Tm Yb Lu
b)
SK12-216 (n=29)
12 similar trend samples
15.4 ± 1.2 Ma (MSWD=3.4)
22.3 ± 0.7 (MSWD=2.6)
100µm
SK12-216
young
old
c)
sample 13-26 (n=41)
12.4 ± 5 Ma (MSWD=0.8)
50µm
Nd
8 similar trend samples
13-26

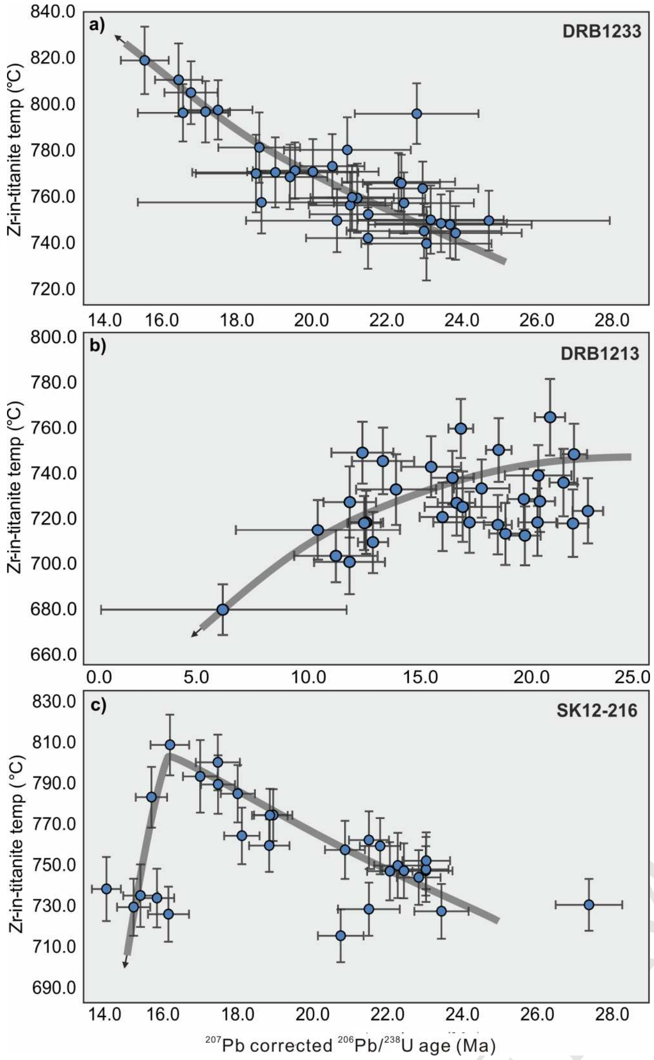

a)
DRB1233
b)
DRB1213
c)
SK12-216
Zr-in-titanite temp (°C)
207Pb corrected 206Pb/238U age (Ma)

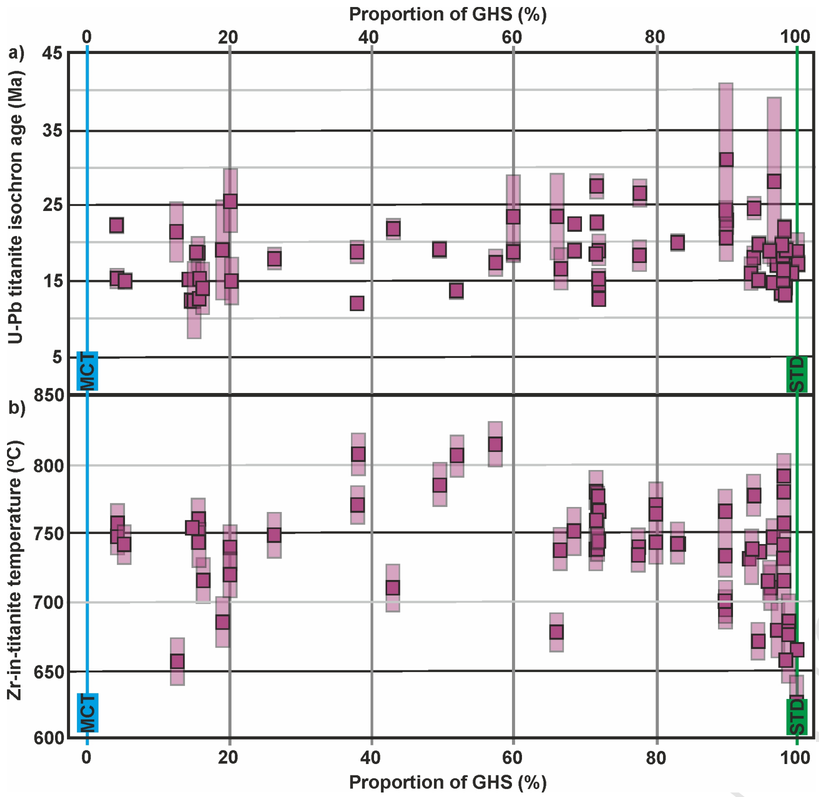

Proportion of GHS (%)
0
20
40
60
80
100
a)
U-Pb titanite isochron age (Ma)
45
35
25
15
5
MCT
STD
b)
Zr-in-titanite temperature (ºC)
850
800
750
700
650
600
MCT
STD
0
20
40
60
80
100
Proportion of GHS (%)

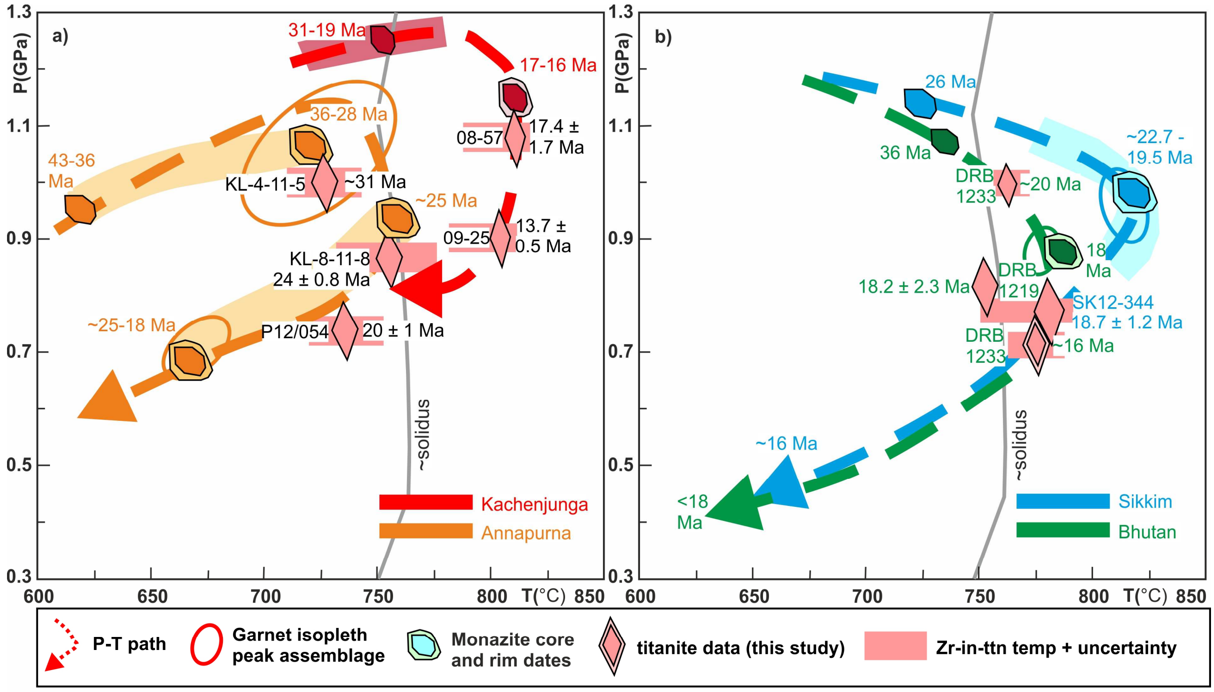

a)
b)
P(GPa)
T(°C)
31-19 Ma
17-16 Ma
36-28 Ma
43-36 Ma
08-57
17.4 ± 1.7 Ma
KL-4-11-5
~31 Ma
~25 Ma
09-25
13.7 ± 0.5 Ma
KL-8-11-8
24 ± 0.8 Ma
~25-18 Ma
P12/054
20 ± 1 Ma
~solidus
Kachenjunga
Annapurna
26 Ma
36 Ma
~22.7 - 19.5 Ma
DRB 1233
~20 Ma
18 Ma
DRB 1219
18.2 ± 2.3 Ma
SK12-344
18.7 ± 1.2 Ma
DRB 1233
~16 Ma
~16 Ma
<18 Ma
Sikkim
Bhutan
P-T path
Garnet isopleth peak assemblage
Monazite core and rim dates
titanite data (this study)
Zr-in-ttn temp + uncertainty

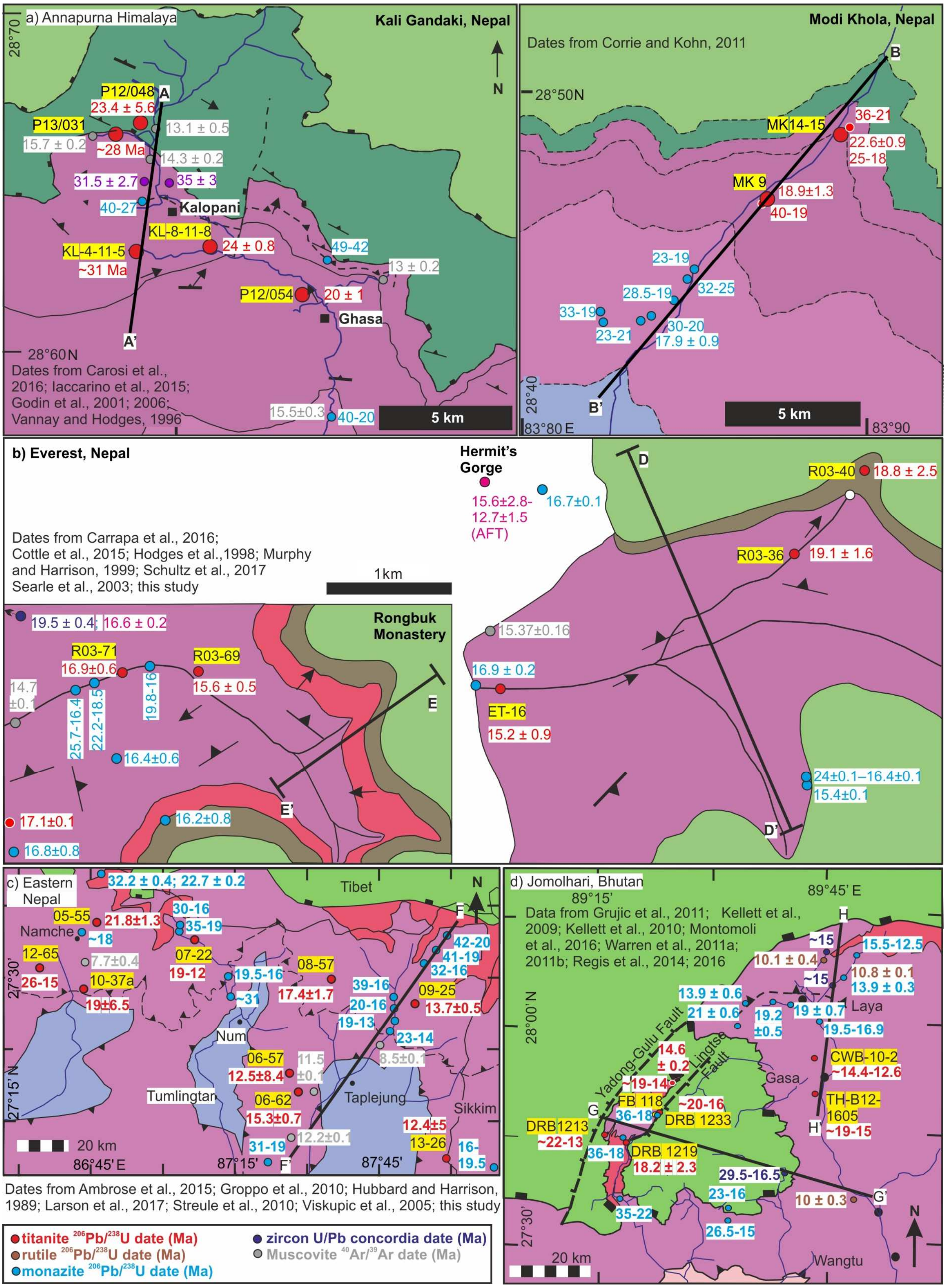
a) Annapurna Himalaya
Kali Gandaki, Nepal
28°70
N
P12/048
23.4 ± 5.6
P13/031
15.7 ± 0.2
~28 Ma
13.1 ± 0.5
14.3 ± 0.2
31.5 ± 2.7
35 ± 3
40-27
Kalopani
KL-8-11-8
KL-4-11-5
~31 Ma
24 ± 0.8
49-42
13 ± 0.2
P12/054
20 ± 1
Ghasa
A
A'
28°60N
Dates from Carosi et al., 2016; Iaccarino et al., 2015; Godin et al., 2001; 2006; Vannay and Hodges, 1996
15.5±0.3
40-20
5 km
Modi Khola, Nepal
Dates from Corrie and Kohn, 2011
28°50N
B
MK14-15
36-21
22.6±0.9
25-18
MK 9
18.9±1.3
40-19
23-19
28.5-19
32-25
33-19
23-21
30-20
17.9 ± 0.9
28°40
83°80 E
B'
5 km
83°90
b) Everest, Nepal
Hermit's Gorge
15.6±2.8-12.7±1.5 (AFT)
16.7±0.1
Dates from Carrapa et al., 2016; Cottle et al., 2015; Hodges et al.,1998; Murphy and Harrison, 1999; Schultz et al., 2017 Searle et al., 2003; this study
1km
D
R03-40
18.8 ± 2.5
R03-36
19.1 ± 1.6
19.5 ± 0.4; 16.6 ± 0.2
Rongbuk Monastery
R03-71
16.9±0.6
R03-69
15.6 ± 0.5
14.7 ±0.1
25.7-16.4
22.2-18.5
19.8-16
16.4±0.6
E
E'
17.1±0.1
16.2±0.8
16.8±0.8
15.37±0.16
16.9 ± 0.2
ET-16
15.2 ± 0.9
24±0.1–16.4±0.1
15.4±0.1
D'
c) Eastern Nepal
32.2 ± 0.4; 22.7 ± 0.2
Tibet
N
F
05-55
21.8±1.3
30-16
35-19
Namche
~18
07-22
19-12
12-65
26-15
7.7±0.4
10-37a
19±6.5
27°30'
19.5-16
~31
08-57
17.4±1.7
42-20
41-19
32-16
39-16
20-16
19-13
09-25
13.7±0.5
23-14
Num
06-57
12.5±8.4
11.5 ±0.1
8.5±0.1
Tumlingtar
06-62
15.3±0.7
Taplejung
Sikkim
27°15' N
12.2±0.1
12.4±5
13-26
16-19.5
31-19
20 km
86°45'E
87°15'
87°45'
F'
d) Jomolhari, Bhutan
89°15'
89°45' E
Data from Grujic et al., 2011; Kellett et al., 2009; Kellett et al., 2010; Montomoli et al., 2016; Warren et al., 2011a; 2011b; Regis et al., 2014; 2016
H
~15
15.5-12.5
10.1 ± 0.4
~15
10.8 ± 0.1
13.9 ± 0.3
28°00'N
13.9 ± 0.6
21 ± 0.6
19.2 ±0.5
19 ± 0.7
Laya
19.5-16.9
14.6 ± 0.2
~19-14
Yadong-Gulu Fault
Lingtse Fault
Gasa
CWB-10-2
~14.4-12.6
TH-B12-1605
~19-15
G
FB 118
36-18
~20-16
DRB 1233
DRB1213
~22-13
H'
36-18
DRB 1219
18.2 ± 2.3
29.5-16.5
23-16
G'
10 ± 0.3
35-22
26.5-15
27°30'
20 km
N
Wangtu
Dates from Ambrose et al., 2015; Groppo et al., 2010; Hubbard and Harrison, 1989; Larson et al., 2017; Streule et al., 2010; Viskupic et al., 2005; this study
titanite 206Pb/238U date (Ma)
rutile 206Pb/238U date (Ma)
monazite 206Pb/238U date (Ma)
zircon U/Pb concordia date (Ma)
Muscovite 40Ar/39Ar date (Ma)

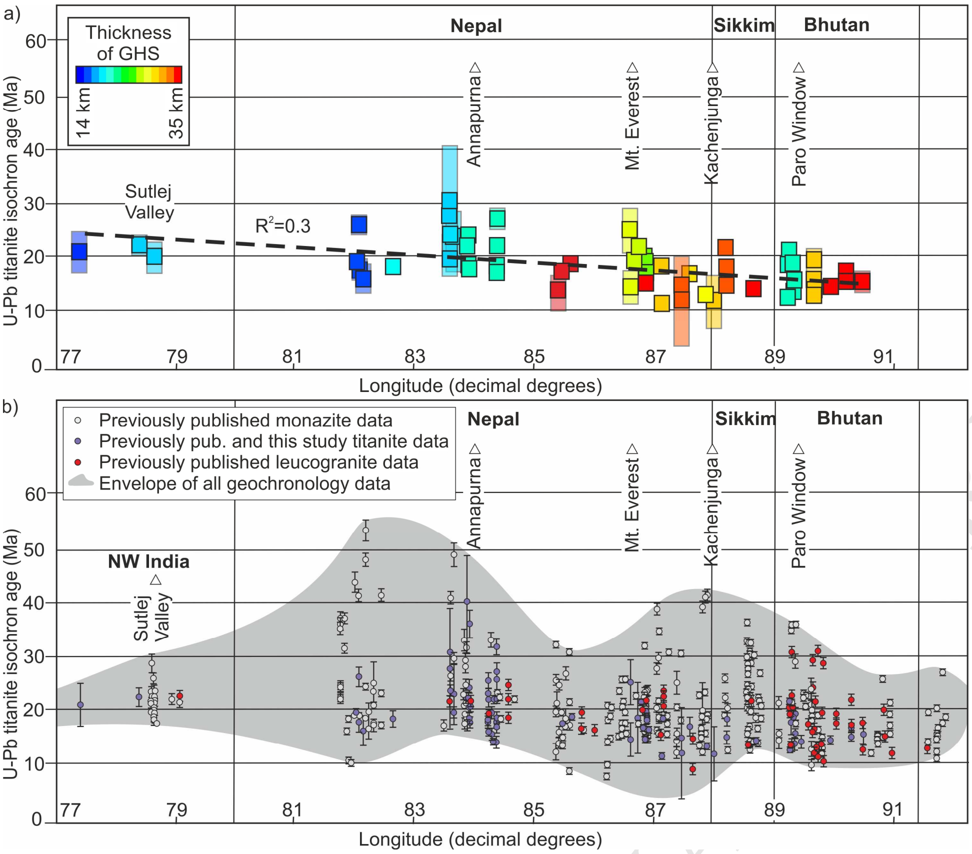
a)
Thickness of GHS
14 km
35 km
Nepal
Sikkim
Bhutan
Annapurna
Mt. Everest
Kachenjunga
Paro Window
Sutlej Valley
R²=0.3
U-Pb titanite isochron age (Ma)
Longitude (decimal degrees)
b)
Previously published monazite data
Previously pub. and this study titanite data
Previously published leucogranite data
Envelope of all geochronology data
NW India
Sutlej Valley
Nepal
Sikkim
Bhutan
Annapurna
Mt. Everest
Kachenjunga
Paro Window
U-Pb titanite isochron age (Ma)
Longitude (decimal degrees)

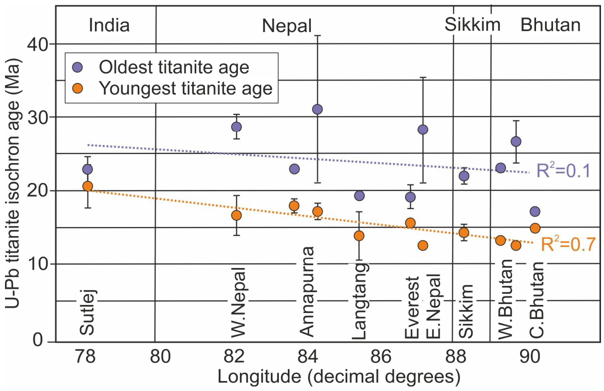
India
Nepal
Sikkim
Bhutan
Oldest titanite age
Youngest titanite age
U-Pb titanite isochron age (Ma)
40
30
20
10
0
R^2=0.1
R^2=0.7
Sutlej
W.Nepal
Annapurna
Langtang
Everest
E.Nepal
Sikkim
W.Bhutan
C.Bhutan
78
80
82
84
86
88
90
Longitude (decimal degrees)

Campaign-style U-Pb titanite petrochronology; along-strike variations in timing of metamorphism in the Himalayan Metamorphic Core.

Catherine M. Mottram[1], John Cottle[2], and Andrew Kylander-Clark[2]

[1]*School of Earth and Environmental Sciences, University of Portsmouth, Portsmouth, U.K.*

catherine.mottram@port.ac.uk

[2]*Department of Earth Science, University of California, Santa Barbara, 93106-9630, United States*

Highlights

- Investigation of along-strike variations in the Himalayan mountain belt
- Campaign-style titanite petrochronology study analyzing 47 samples from >2000 km
- Results show eastward younging in titanite ages
- Younger, thicker and hotter core of the mountain belt in the east
- Accretion and duplexing along the basal detachment control along-strike trends